nature communications

Article

https://doi.org/10.1038/s41467-025-62788-6

A citrullinated histone H3 monoclonal antibody for immune modulation in sepsis

Received: 13 January 2025

Accepted: 29 July 2025

Published online: 12 August 2025

Check for updates

Wenlu Ouyang[1,2], Yuchen Chen[3], Tao Tan[3], Yujing Song[4,5], Tao Dong[1,6], Xin Yu[1,7], Kyung Eun Lee[3], Xinyu Zhou[3], Zoe Tetz[3], Sophia Go[3], Xindi Zeng[3], Liujiazi Shao[1], Chao Quan[1,8], Ting Zhao[9], Yuzi Tian[1,10], Katsuo Kurabayashi[4,5,11], Hua Jin[12], Jichun Ma[12], Jingdong Qin[12], Brandon Williams[12], Qingtian Li[12], Gui-dong Zhu[12], Hasan B. Alam[13], Kathleen A. Stringer[14,15,16], Yongqing Li[1] ✉ & Jianjie Ma[3] ✉

Citrullinated histone H3 (CitH3), released from immune cells during early sepsis, drives a vicious cycle of inflammation through excessive NETosis and pyroptosis, causing immune dysfunction and tissue damage. To regulate this process, we develop a humanized CitH3 monoclonal antibody (hCitH3-mAb) with high affinity and specificity to target this process. In murine models, hCitH3-mAb reduces cytokine production, mortality and acute lung injury (ALI) caused by LPS and *Pseudomonas aeruginosa* while enhancing bacteria phagocytosis in the lungs, spleen, and liver. Using pre-equilibrium digital ELISA (PEdELISA), we identify an optimal therapeutic window for hCitH3-mAb in sepsis-induced ALI. In parallel, we explore the molecular mechanism underlying CitH3-driven inflammation. We find that in macrophages, CitH3 activates Toll-like receptor 2 (TLR2), triggering Ca^{2+}-dependent PAD2 auto-citrullination and nuclear translocation, amplifying CitH3 production via a harmful feedback loop. The hCitH3-mAb treatment effectively disrupts this cycle and restores macrophage function under septic conditions. Together, these findings highlight both the therapeutic potential of hCitH3-mAb and provide a deep mechanistic insight into the CitH3–PAD2 axis in sepsis, supporting its further development for treating immune-mediated diseases.

Sepsis is a life-threatening condition caused by a dysregulated immune response to infection, resulting in organ dysfunction and high mortality rates[1,2]. Clinically, sepsis often leads to severe complications such as acute lung injury (ALI) or acute respiratory distress syndrome (ARDS), renal failure, and coagulopathies, which significantly worsen prognosis[3,4]. A hallmark of sepsis is the cytokine storm, an overwhelming release of pro-inflammatory cytokines that drives hyperinflammation, tissue damage and organ failure[5,6]. Despite advances in medical care, there are no real-time tools to monitor this storm, and current treatments remain ineffective in controlling immune dysregulation[7], highlighting the urgent need for novel therapeutic strategies.

Immune dysregulation in sepsis involves key players such as neutrophils and macrophages[8,9]. While neutrophil extracellular traps (NETs) are essential for pathogen control[10–16], excessive NETosis contributes to inflammation and tissue injury[10,17–22]. Similarly, macrophage dysfunction, exacerbated by pyroptosis, a form of programmed cell death involving caspase activation, impairs pathogen clearance, fueling persistent infections and immune collapse[23–25]. Targeting excessive NETosis while preserving NETs' beneficial functions and restoring macrophage activity represents a promising therapeutic approach.

Citrullinated histone H3 (CitH3), a key component released during NETosis, has emerged as a critical mediator in sepsis pathology[26]. Generated by the post-translational modification of histone H3 by

A full list of affiliations appears at the end of the paper. ✉e-mail: yqli@med.umich.edu; Jianjie.ma@virginia.edu

https://doi.org/10.1038/s41467-025-62788-6

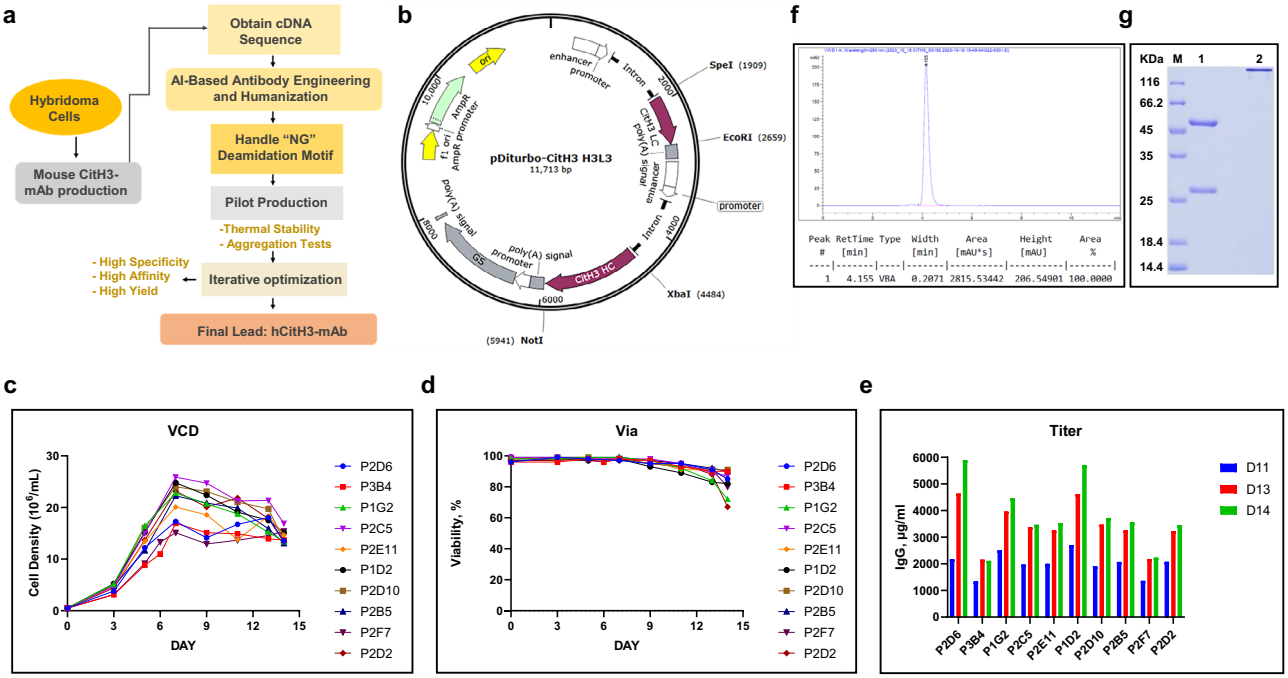

Fig. 1 | Thematic approach for the optimization and scale-up production of hCitH3-mAb. a Schematic flowchart illustrating the humanization process of mouse CitH3-mAb and the optimization steps conducted during developability studies, culminating in the scale-up production of hCitH3-mAb. **b** Plasmid map detailing the co-expression of the heavy chain and light chain of hCitH3-mAb in CHO cells. **c** Quantification of cell density for different stable CHO clones expressing hCitH3-mAb. **d** Assessment of cell viability across the various CHO clones stably expressing hCitH3-mAb.**e**, Titer quantification of stable CHO clones, highlighting clone P2D6, which exhibited the highest hCitH3-mAb titers on days 13 and 14. Clone P2D6 was selected for harvesting and purification. **f** RF-HPLC analysis demonstrated a homogeneous distribution of the purified hCitH3-mAb, achieving >99.5% purity (dominant peak) with no detectable aggregation. **g** SDS-PAGE analysis of purified hCitH3-mAb revealed a distinct heavy chain and light chain under reducing conditions, and a single band under non-reducing conditions, indicating high purity and proper assembly. For every batch of the hCitH3-mAb, such quality control assessment is routinely performed by CDMO. Similar results were obtained from ≥3 independent replicates.Source data are provided as a Source Data file.

peptidyl arginine deiminases (PADs), particularly PAD2 and PAD4[27,28], CitH3 amplifies inflammation and immune dysfunction. We and others have shown that CitH3 is a promising biomarker for early diagnosis of sepsis and related conditions[29–31]. While PAD4 is predominantly localized in the nucleus, PAD2 has the capacity to translocate from the cytosol to the nucleus under stress conditions to facilitate CitH3 production[32–36]. However, the mechanisms driving PAD2's nuclear translocation during immune responses remain poorly understood.

Recent findings from our laboratory demonstrate that PAD2-knockout mice exhibit significantly improved survival under septic conditions compared to their wild-type littermates, whereas PAD4-knockout mice show only marginal improvement[37–39]. These results suggest that PAD2 plays a pivotal role in regulating CitH3 production and NETosis in sepsis, emphasizing the need to elucidate the mechanistic basis of PAD2 nuclear translocation and its interaction with histone H3 substrates.

Elevated CitH3 are believed to perpetuate a vicious cycle of inflammation by driving excessive NETosis and pyroptosis, thereby exacerbating immune dysfunction and tissue damage[27,37,40,41]. Despite its central role in sepsis pathology, the mechanisms underlying the initiation of CitH3 signaling and its intracellular pathway remain poorly understood, creating a significant barrier to therapeutic intervention.

Studying CitH3 signaling requires a highly specific, high-affinity anti-CitH3 monoclonal antibody (mAb) with robust CitH3-neutralizing capability. However, existing commercial antibodies predominantly target citrullinated residues at R2, R8, and R17 of histone H3, which are catalyzed by PAD4 but not PAD2, limiting their effectiveness in neutralizing CitH3[33,42,43]. To address this limitation, we previously developed a mouse-derived CitH3-mAb that targets citrullinated H3 at R2, R8, R17 and R26[40]. This CitH3-mAb effectively binds CitH3 catalyzed by both PAD2 and PAD4, demonstrating therapeutic potential in sepsis models. However, the murine origin of these antibodies limits their clinical application, necessitating the development of a humanized version for therapeutic use.

In this study, we report the development and preclinical evaluation of a novel humanized anti-CitH3 monoclonal antibody (hCitH3-mAb), which retains high affinity and broad specificity for PAD2- and PAD4-mediated CitH3 in animal models of sepsis. We focus on its ability to disrupt CitH3-driven feedback loops, mitigate the inflammatory cytokines, restore macrophage function, and protect against sepsis-induced pulmonary injury. In addition, we investigate the underlying mechanism of CitH3-mediated immune activation and uncover a feedback loop involving TLR2 activation and Ca^{2+}-dependent PAD2 auto-citrullination and nuclear translocation, which sustains and amplifies CitH3 production. Together, our findings position hCitH3-mAb as both a mechanistic probe and a transformative therapeutic candidate for sepsis and other inflammatory diseases, addressing critical gaps in immune regulation and disease management.

Results

A thematic approach to achieve optimization of the humanized CitH3 monoclonal antibody

To create the humanized hCitH3-mAb from the original mouse antibody[40], a multi-step approach was used to maintain binding specificity while reducing immunogenicity for human use (Fig. 1). The process began with isolating RNA from mouse hybridoma cells secreting the CitH3-mAb, which was then reverse-transcribed into cDNA. This cDNA sequence served as the blueprint for humanization using AI-driven monoclonal antibody engineering (Fig. 1a). This advanced technique helped select human framework sequences that retained the original antibody's binding specificity to the CitH3 peptide, targeting citrulline residues at histone positions 2, 8, 17, and 26.

https://doi.org/10.1038/s41467-025-62788-6

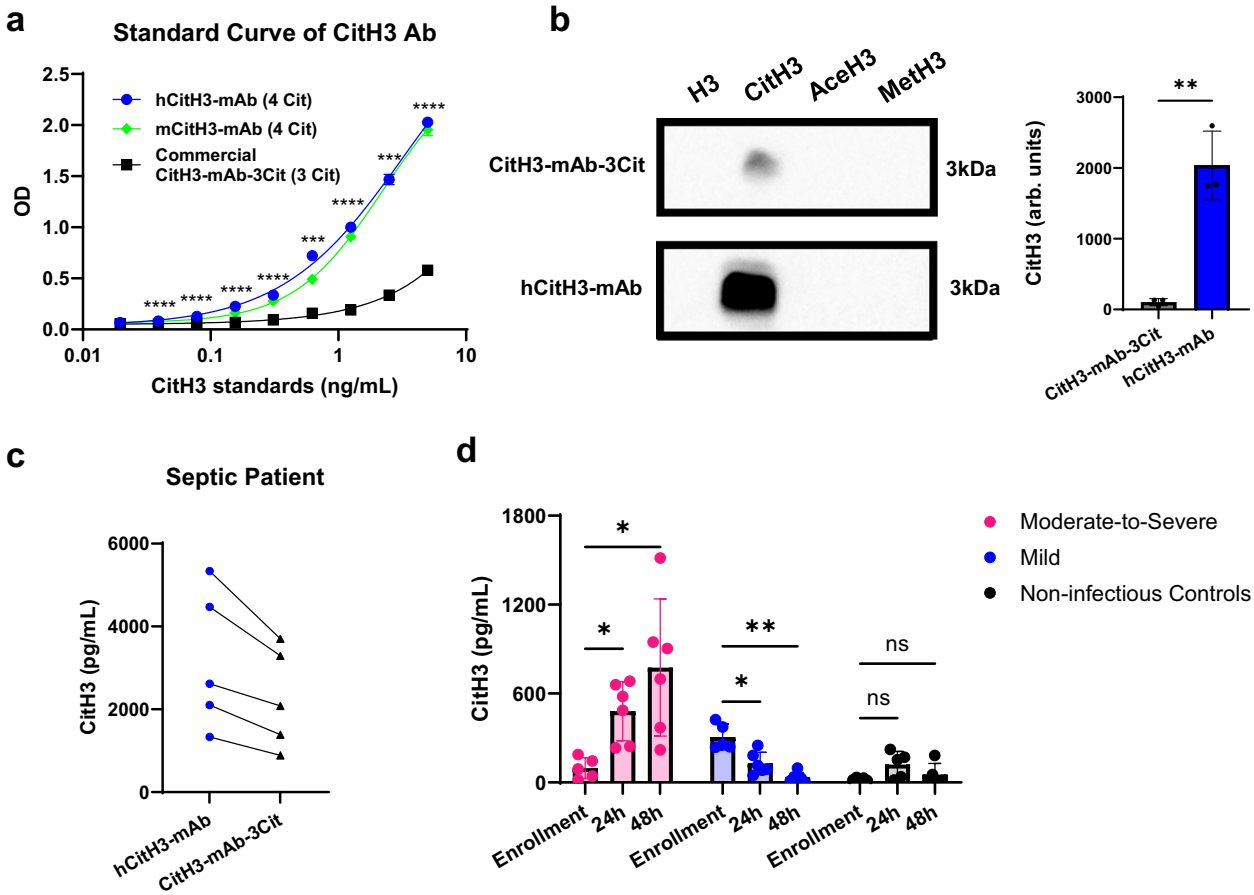

Fig. 2 | hCitH3-mAb exhibits superior binding capacity to CitH3 compared to commercial CitH3 antibodies. a Indirect ELISA quantification demonstrating the sensitivity of hCitH3-mAb (blue) versus commercial CitH3-mAb-3Cit antibodies (black). CitH3 standards and test samples were identically diluted, and ELISA procedures were performed in parallel under identical conditions ($n = 3$). Statistical significance was analyzed using two-way ANOVA (two-sided). ***$p < 0.001$, ****$p < 0.0001$. The asterisks in the figure indicate comparisons between hCitH3-mAb and commercial CitH3-mAb-3Cit antibodies. **b** Western blot analysis comparing the sensitivity and specificity of hCitH3-mAb and CitH3-mAb-3Cit. Four peptides (H3, CitH3 (R2,8,17,26), AceH3, and MetH3)were each loaded at 0.5 μg. After electrophoresis and membrane transfer, the blot was divided and probed separately with either hCitH3-mAb or CitH3-mAb-3Cit (2 μg/L). Membranes were processed and exposed simultaneously ($n = 3$ independent experiments). Data are presented as mean ± SD. Statistical analysis was performed using a two-sided t-test (**$p < 0.01$). **c** ELISA of human septic serum samples, comparing the sensitivity of hCitH3-mAb and CitH3-mAb-3Cit. **d** ELISA quantification of CitH3 protein levels in human serum samples. Serum was collected from patients at enrollment, at 24- and 48 h post-enrollment. For the infectious groups, $n = 6$ at both 24- and 48 h; for the other group, $n = 5$. The 'Mild' group corresponds to patients with a total SOFA score ≤6, while the 'Moderate-to-Severe' group corresponds to a SOFA score >6. Non-infectious controls represent patients who experience shock without clinical or laboratory evidence of infection. Data are presented as mean ± SD. Statistical significance was determined using two-way ANOVA with Turkey's multiple comparisons test (*$p < 0.05$, **$p < 0.01$).Source data are provided as a Source Data file.

A crucial modification during this process was the removal of the "NG" amidation motif found in the HCDR2 and LCDR1 domains, which was achieved by substituting glycine with alanine. This change enhanced the antibody's stability and improved scalability for large-scale manufacturing. Bon Opus Biosciences played a pivotal role in the design and optimization of expression vectors for hCitH3-mAb. By co-transfecting various heavy (VH) and light (VL) chain combinations into CHO cells, they identified configurations that yielded the highest binding activity and antibody production (Fig. 1b). This detailed engineering process resulted in a stable, high-affinity humanized antibody, positioning it well for further therapeutic development.

Subsequently, in collaboration with SparX Biopharmaceutical Corp, a comprehensive developability study was conducted using CHO-GS KO cells. After electroporating the plasmid into CHO cells, single-cell dilution and screening enabled the selection of clones with high-titer expression of hCitH3-mAb. Notably, clones P2D6 and P1D2 demonstrated robust cell density (Fig. 1c) and viability (Fig. 1d), achieving impressive titers of 6–8 g/L at day 14 in culture (Fig. 1e).

Highly purified hCitH3-mAb was obtained from these CHO clones via Protein A-chromatography, with > 99.5% purity (Fig. 1f). Furthermore, hCitH3-mAb demonstrated high thermal stability and minimal aggregation (< 0.5%) based on SEC-HPLC analysis (Fig. 1g), underscoring its suitability for scalable production and clinical application.

hCitH3-mAb exhibits superior binding capacity to CitH3 compared to commercial CitH3-mAb

We evaluated the specificity and bioactivity of hCitH3-mAb using immunoblotting and ELISA assays. In the ELISA assay (Fig. 2a), hCitH3-mAb demonstrated a higher optical density (OD, blue symbol) than the commercial CitH3 antibodies (black symbol), which primarily recognize PAD4-mediated citrullination of H3 at R2, R8 and R17 (referred to as CitH3-mAb-3Cit). This increased OD was observed across a range of CitH3 peptide concentrations, indicating a clear dose-response relationship. Notably, hCitH3-mAb exhibited a lower limit of detection (LOD) and a higher signal-to-noise ratio (SNR) in the standard curve,

https://doi.org/10.1038/s41467-025-62788-6

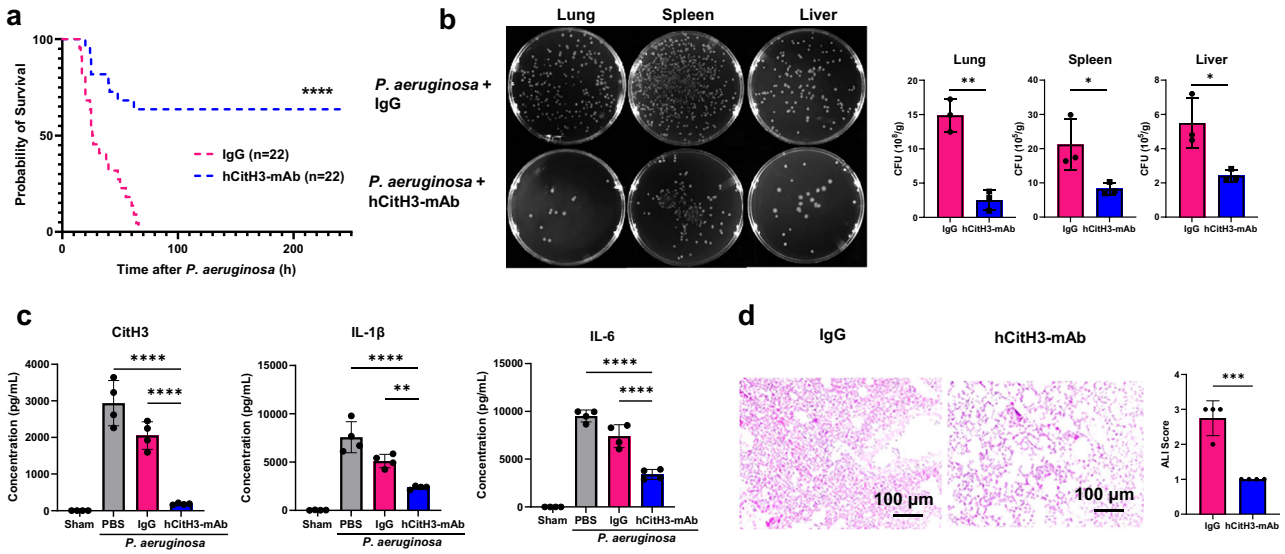

Fig. 3 | hCitH3-mAb reduces inflammation and protects against sepsis-induced ALI in mice. a Kaplan-Meier curves of mice after administration of *Pseudomonas aeruginosa* (*P. aeruginosa*, 2.5×10^6 CFU) for 10 days. Mice were divided into two groups: one receiving hCitH3-mAb (20 mg/kg) and the other receiving human IgG, with treatments administered within 30 min of sepsis onset. Data represent pooled results from three independent experiments (total $n = 22$; 6–8 mice per group per experiment). **b** Bacterial load in the lung, spleen, and liver 24 h after *P. aeruginosa* inoculation in mice treated with either hCitH3-mAb or human IgG ($n = 3$ per group). Homogenized organs were weighed, serially diluted, and plated on nutrient agar plates. Colony counts were obtained using ImageJ after 16-hour incubation at 37 °C. Data are presented as mean ± SD. **c** Levels of CitH3, IL-1β, and IL-6 in bronchoalveolar lavage fluid (BALF) from mice treated with hCitH3-mAb, compared to those treated with PBS or human IgG ($n = 4$ per group). Data are presented as mean ± SD. **d** Representative images and assessment of lung tissue sections stained with H&E. ALI scores and the proportion of airspace area were quantified by a blinded pathologist ($n = 4$ per group). Data are presented as mean ± SD. Statistical analyses were performed using Kaplan-Meier analysis with two-sided log-rank test for (**a**), two-sided t-tests for (**b**, **d**), and one-way ANOVA with Dunnett's multiple comparisons test for (**c**): $^*p < 0.05$, $^{**}p < 0.01$, $^{***}p < 0.001$, $^{****}p < 0.0001$.Source data are provided as a Source Data file.

highlighting its higher sensitivity in detecting CitH3 and its lower matrix effect (**See Source Data of Fig.2a**).

To include additional antibodies, we also performed a direct ELISA by coating the CitH3 antigen onto plates and directly conjugating HRP to each antibody (Supplementary Fig. 1, Supplementary Table 1 and Supplementary Table 2). This approach allowed us to evaluate a broader range of commercial antibodies, independent of isotype compatibility with the secondary detection system. Under the same experimental conditions, hCitH3-mAb exhibited the lowest LOD, the highest SNR, and the lowest EC_{50}, further confirming its superior sensitivity and binding affinity.

Immunoblotting was conducted using both the commercial CitH3-mAb-3Cit and our hCiitH3-mAb under identical experimental conditions, including antibody concentration, incubation time, and exposure duration (Fig. 2b). Clearly, both hCitH3-mAb and CitH3 mAb-3Cit displayed high specificity for the CitH3 peptide, with no detection of bands for non-modified H3, acetylated H3 (AceH3), or methylated H3 (MetH3). Moreover, a greater than 100-fold higher signal was observed for our hCitH3-mAb than the commercial CitH3-mAb-3Cit.

Previously, we reported elevated circulating CitH3 levels in patients with septic shock, which correlated with greater disease severity and suggested its potential as a biomarker[31,41,44]. To further evaluate detection performance, we quantified CitH3 protein levels in serum samples collected from septic patients using hCitH3-mAb and a commercial CitH3-mAb (Fig. 2c). Clearly, hCitH3-mAb detected the higher levels of CitH3 in serum samples derived from septic patients, compared with the commercial CitH3-mAb-3Cit antibody. Data were grouped based on Sequential Organ Failure Assessment (SOFA) score. As shown in Fig. 2d, septic patients exhibited elevated serum CitH3 levels within 1 h of diagnosis. In septic patients with moderate-to-severe dysfunction (total SOFA score >6), CitH3 levels continued to rise at 24 and 48 h post-diagnosis, whereas surviving patients with mild dysfunction (total SOFA score ≤6) demonstrated declining CitH3 levels over the same period. In contrast, serum samples from non-sepsis ALI patients displayed low CitH3 levels, indistinguishable from those of healthy volunteers. These results support the potential of hCitH3-mAb in diagnostic applications for sepsis.

These findings highlight the superior sensitivity of hCitH3-mAb in detecting CitH3 compared to commercial antibodies, which is driven by its enhanced binding capabilities and specificity with minimal cross-reactivity with other histone proteins, relative to commercial CitH3-mAb-3Cit antibodies.

hCitH3-mAb reduces inflammation and protects against sepsis-induced ALI

We conducted a comprehensive assessment of hCitH3-mAb's therapeutic potential in a murine model of sepsis. Sepsis was induced by intranasal inoculation of 2.5×10^6 CFU of *Pseudomonas aeruginosa* bacteria, followed by a single intravenous dose of hCitH3-mAb (20 mg/kg, tail vein injection as described before[40]). To control for potential non-specific effects, a parallel cohort received human IgG isotype control. Survival was monitored over a span of 10 days (Fig. 3a, Supplementary Fig. 2a). Notably, hCitH3-mAb treatment significantly increased the survival rate of septic mice compared to the IgG isotype-treated group.

In a separate cohort, tissues and organ samples of septic mice were collected 24 h post-*P. aeruginosa* treatment to assess the therapeutic effects of hCitH3-mAb. Bacteria dissemination during sepsis leads to severe end-organ dysfunction, emphasizing the importance of monitoring bacterial burden. To quantify bacteria load, vital organs were homogenized and analyzed. Notably, hCitH3-mAb treatment resulted in a significant reduction in bacterial burden across key organs, including the lungs, spleen, and liver, compared to the IgG-treated group (Fig. 3b, see also Supplementary Fig. 2c).

Additionally, septic mice exhibited elevated levels of pro-inflammatory cytokines in bronchoalveolar lavage fluid (BALF). Treatment with hCitH3-mAb significantly reduced IL-6 and IL-1β levels in BALF, alongside decreased CitH3 levels, compared to both *P.*

aeruginosa + PBS and *P. aeruginosa* + IgG groups (Fig. 3c). Given that ALI is a major cause of mortality in sepsis, we also examined lung histopathology 24 h post-*P. aeruginosa* induction. Hematoxylin and eosin (H&E) staining (Fig. 3d) unveiled typical inflammatory alterations in IgG-treated animals, including inflammatory infiltrates, pulmonary congestion, edema, alveolar hemorrhage, and thickened alveolar walls. In contrast, lungs from hCitH3-mAb treated mice showed relatively preserved lung structure (see Supplementary Fig. 2d). Quantitative evaluation by a blinded pathologist further confirmed a significant reduction in ALI severity in the hCitH3-mAb treated group, underscoring the protective effects of hCitH3-mAb against *P. aeruginosa*-induced damage.

To assess safety, a high dose of hCitH3-mAb (30 mg/kg, tail vein injection) was systemically administered to C57BL6 mice (both male and females, 3–4 months). Treated mice displayed normal behavior and body weight, indicating the safety nature of the antibody in rodents. In separate experiments, we evaluated tolerability with repetitive dosing of the mouse CitH3-mAb (precursor to hCitH3-mAb). This approach was chosen to mitigate any immune response against hCitH3-mAb. Mice received 10 mg/kg CitH3-mAb injections twice weekly via tail vein for six weeks. The treated mice tolerated this dosing regimen well, with no differences in body weight compared to control groups (Fig. 4a). Echocardiography confirmed that repetitive dosing of CitH3-mAb did not impact cardiac function (Fig. 4b). Blood chemistry analyses showed normal levels of biomarkers for organ functions - blood urine nitrogen (BUN), total protein, globulin, albumin/globulin ratio, alanine aminotransferase (ALT), alkaline phosphatase (ALKP), and non-fasting glucose in serum from mice with or without treatment of hCitH3-mAb Fig. 4c), and the creatinine levels are <0.4 mg/dL in all control and treated mice. Histological assessments of vital organs (heart, liver, kidney, lung and spleen) revealed no abnormalities (Fig. 4d).

The potential antibody-dependent cellular cytotoxicity (ADCC) activity of hCitH3-mAb was evaluated in THP-1 cells using both a peripheral blood mononuclear cell (PBMC) system and a reporter system as part of a safety control assessment to evaluate its potential cytotoxic effects driven by the IgG format (Fig. 4e). In both assay formats, hCitH3-mAb exhibited no detectable ADCC activity. Consistently, the IgG isotype control also showed no ADCC activity, while another positive control a-PDL1 (anti PD-L1 antibody) showed ADCC activity in PD-L1-overexpressing THP-1 cells, together reinforcing the conclusion that hCitH3-mAb does not trigger antibody-dependent cellular cytotoxicity under the tested conditions.

We have partnered with a contract research organization (CRO) and completed the GLP-toxicology study of hCitH3-mAb in rats and monkeys per FDA guidance. These studies have yielded encouraging no-observed-adverse-effect level (NOAEL) data, supporting the favorable safety profile of hCitH3-mAb. Cynomolgus monkey and Sprague Dawley (SD) rat received 4-week repeated intravenous (IV) dosing followed by a 4-week recovery phase. In both models, hCitH3-mAb was well tolerated at all tested doses (30 mg/kg, 90 mg/kg and 200 mg/kg), with no significant toxicity observed. The NOAEL was determined to be 200 mg/kg.

These results demonstrate that hCitH3-mAb is well tolerated in both species, providing strong support for its continued development toward clinical trials. Additionally, as part of these GLP toxicology studies, we have also characterized the pharmacokinetic (PK) properties of hCitH3-mAb in monkeys, with observed half-life typical of other therapeutic monoclonal antibodies (Fig. 4f).

Overall, these findings demonstrate hCitH3-mAb is both safe and effective in protecting mice from consequences of sepsis. Treatment with hCitH3-mAb also significantly improved survival, reduced bacteria load, suppressed pro-inflammatory cytokines and protected against ALI, highlighting its potential as a promising therapeutic strategy for sepsis management.

CitH3 quantification reveals a critical window for sepsis management

Sepsis is a severe and rapidly progressing condition with a high mortality rate[45]. Early intervention is crucial, demanding real-time monitoring of sepsis progression to identify a therapeutic window. Our PEdELISA platform provides a means to efficiently quantify biomarkers for cytokine storms and to track sepsis progression[46–48]. Compared to conventional ELISA, PEdELISA offers greater efficiency and ease (see Supplementary Fig. 3), allowing the quantification of six cytokines from just a drop of plasma within a two-hour timeframe (see Supplementary Fig. 3c). The robust linear correlation between PEdELISA and traditional ELISA validates its reliability (Supplementary Fig. 3b).

In addition to the *P. aeruginosa*-sepsis model (Fig. 3), we have established a LPS endotoxemia model, by administering a lethal dose of LPS (25 mg/kg LPS, intraperitoneal) to C57BL6 mice. The animals were divided into two groups: one receiving hCitH3-mAb (20 mg/kg, tail vein) and the other human IgG as a control. At this lethal LPS dose, 100% mortality was observed within 24 h in the IgG-treated C57BL6/J mice, while the administration of hCitH3-mAb (20 mg/kg) significantly improved survival (Fig. 5a, see also Supplementary Fig. 2b).

Using the compact PEdELISA platform with hCitH3-mAb, we detected a biphasic elevation of CitH3 in LPS-induced endotoxemia in mice (Fig. 5b, c). CitH3 levels began to rise as early as three hours post-LPS administration, continuing to increase over the 21 h observation window. A more pronounced elevation in CitH3 was observed around 18 h post-exposure (Fig. 5c). Remarkably, hCitH3-mAb administration effectively prevented CitH3 elevation and cytokine storm development, likely contributing to the observed survival benefits. These findings suggest a critical threshold level for CitH3 as an early biomarker for sepsis onset, identifying a key therapeutic window prior to the cytokine storm.

To further investigate cytokine dynamics, we expanded PEdELISA's multiplexing capability to assess early LPS-induced cytokine changes (Fig. 5d). Unlike the biphasic CitH3 pattern, IL-1β and IL-6 increased progressively post-LPS exposure, while TNF-α peaked transiently within six hours. These variations limit IL-1β, IL-6, and TNF-α as early sepsis biomarkers. However, combining CitH3 with IL-1β, IL-6, and TNF-α offers a more quantitative assessment of sepsis-associated ALI.

We also examined cytokine patterns in the *P. aeruginosa* infection model (Supplementary Fig. 3). Slightly differing from the LPS model, CitH3, IL-1β, IL-6, and TNF-α levels remained relatively low during the first 12 h post-infection, followed by a more pronounced increase thereafter. This temporal pattern suggests the existence of a therapeutic window in the *P. aeruginosa* model as well, although its timing differs from that observed in the endotoxemia model.

The combination of PEdELISA and CitH3 as a reliable biomarker demonstrates significant clinical translation potential. This fine-time monitoring highlights the critical importance of administering hCitH3-mAb early in sepsis onset to optimize therapeutic efficacy.

Bacteria-infection induced injury to macrophages is protected by hCitH3-mAb

Building on the established therapeutic efficacy of hCitH3-mAb in vivo, we investigated its immunomodulatory mechanisms, particularly focusing on macrophage function. Using THP-1 cells as a macrophage model, we treated THP-1 monocytes with PMA to induce differentiation into macrophages. Exposure of THP-1 macrophages to various doses of *P. aeruginosa* led to dose-dependent cell injury, evidenced by neutral red assay in the culture medium (Supplementary Fig. 4a). Additionally, western blot analysis revealed a time-dependent release of CitH3 protein (17 kD) following *P. aeruginosa* exposure (Fig. 6a), indicating that bacterial infection may prompt CitH3 release and cytokine production, contributing to sepsis-associated immune dysfunction.

https://doi.org/10.1038/s41467-025-62788-6

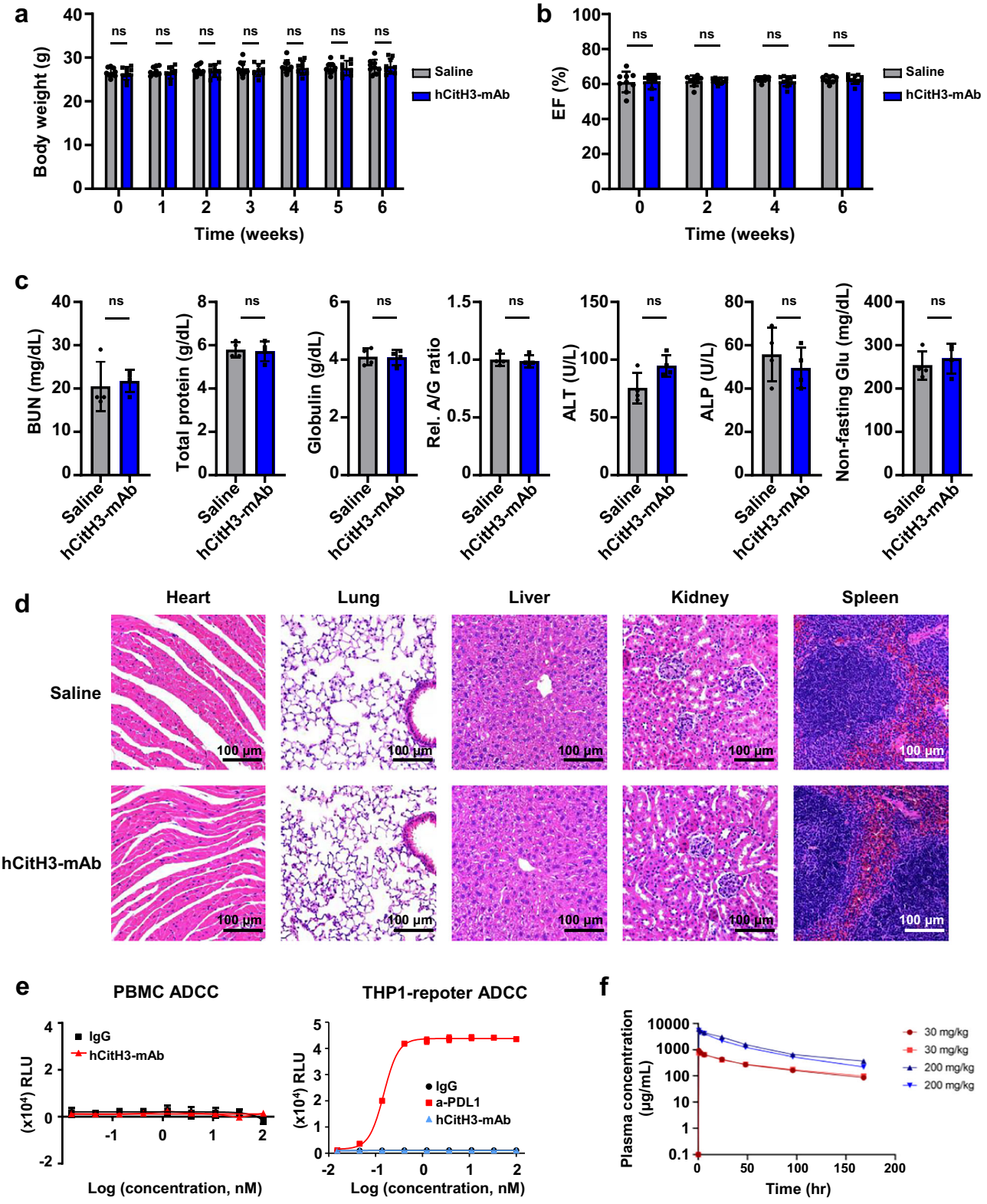

We then examined hCitH3-mAb's potential protective effects on macrophages exposed to *P. aeruginosa*. In THP-1 macrophages challenged with *P. aeruginosa* (MOI = 100), hCitH3-mAb provided dose-dependent protection, while human IgG had no effect on cell viability (Fig. 6b). Phagocytic function was assessed using pHrodo Red *E. coli* BioParticles (Fig. 6c). Notably, *P. aeruginosa* exposure caused extensive macrophage cell death and reduced phagocytic activity with incubation of IgG as control. In contrast, hCitH3-mAb treatment preserved both macrophage viability and phagocytic function.

To further assess macrophage resilience, we treated THP-1 cells with BALF derived from *P. aeruginosa*-exposed septic mice, which contains pro-inflammatory factors. This BALF caused marked cell damage, as indicated by cytoplasmic neoplasm quantification (Fig. 6d). hCitH3-mAb treatment significantly ameliorated these damaging effects, whereas IgG had no impact. Additionally, *P. aeruginosa*-

https://doi.org/10.1038/s41467-025-62788-6

Fig. 4 | Safety profile of CitH3-mAb in C57BL6 mice and negative ADCC effect of hCitH3-mAb. a Body weight of mice before and during the treatment for 6 weeks. Mice were divided into two groups, 9 receiving CitH3-mAb (10 mg/kg) and the other 9 receiving saline, with treatment administrated twice per week ($n = 9$ biological samples per group). **b** Ejection fraction (EF) data of mice treated with CitH3-mAb (10 mg/kg) or saline. Echocardiography assay were conducted before and every two weeks during the treatment ($n = 9$ biological samples per group).**c**, Levels of BUN, total protein, globulin, albumin/globulin ratio, ALT, ALP and non-fasting glucose in serum from mice treated with CitH3-mAb, compared to those treated with saline. Creatinine of all the indicated mice were below 0.4 mg/dL. 4 out of 9 mice in each group were randomly selected for serum chemistry assay and histological analysis ($n = 4$ biological samples per group)**d**, Representative images and assessment of vital organ sections (heart, lung, liver, kidney, spleen) stained with H&E ($n = 4$ per group). **e** ADCC evaluation of hCitH3-mAb in THP-1 cells. PD-L1 transient expression in THP1 cells was used as positive control for ADCC. No ADCC response was observed with hCitH3-mAb ($n = 2$ per group; GLP-compliant study at a certified CRO). **f** Pharmacokinetics of hCitH3-mAb in Cynomolgus monkeys following intravenous infusion. Two doses of hCitH3-mAb (30 or 200 mg/kg) were administered, and the plasma concentrations of the antibody were quantified during the one-week observation time. The estimated half-life was 76.7 and 47.7 h, for 30 mg/kg and 200 mg/kg dosing, respectively. ($n = 2$ per dose group; GLP-compliant study at a certified CRO) Data are presented as mean ± SD. Statistical analysis was performed using two-sided t-tests: ns no significance. Source data are provided as a Source Data file.

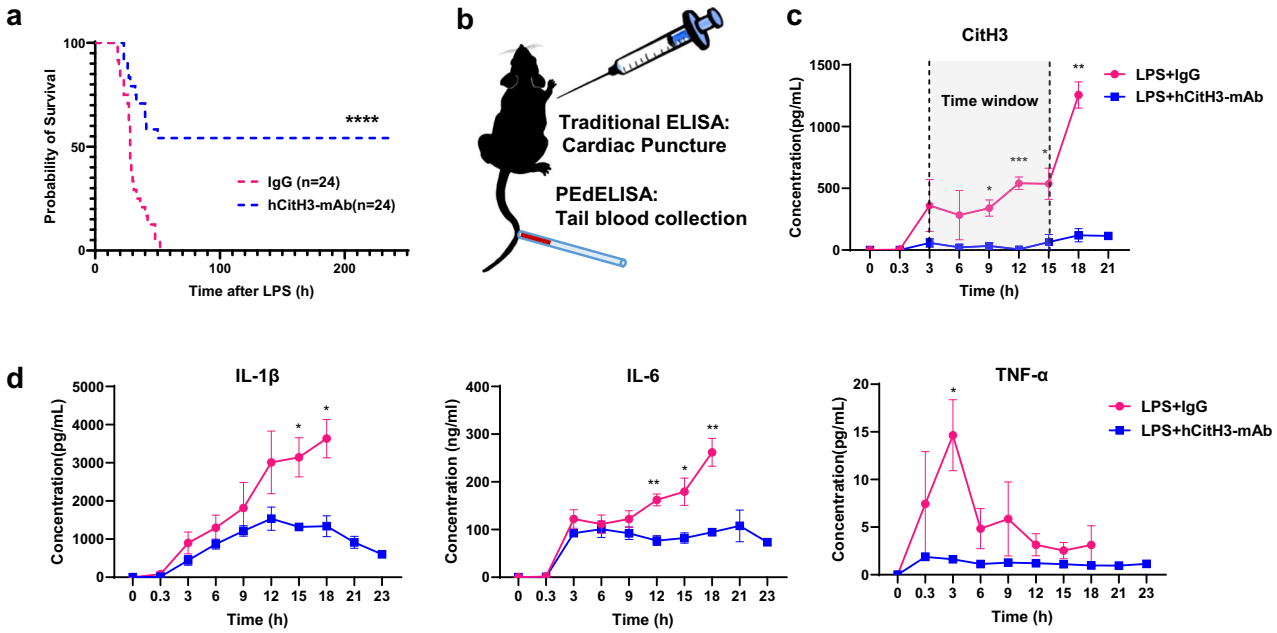

Fig. 5 | hCitH3-mAb protects against LPS-induced endotoxemia in mice by mitigating cytokine storm development. a Kaplan-Meier curves of mice monitored over 10 days following lipopolysaccharide (LPS, 25 mg/kg) administration. Septic mice received hCitH3-mAb (20 mg/kg) or human IgG (20 mg/kg) via tail vein injection 30 min after sepsis onset. Data represent pooled results from three independent experiments (total $n = 24$; 8 mice per group per experiment). **b** Illustration of traditional ELISA and PEdELISA for the detection of cytokines and CitH3. **c** Blood samples were collected at 3 h intervals from the same mouse ($n = 3$ per group) and analyzed using PEdELISA. 8 μL of serum samples were used for CitH3 quantification, revealing a biphasic response of LPS-induced CitH3 elevation indicative of sepsis onset and cytokine storm development. hCitH3-mAb treatment mitigated LPS-induced CitH3 elevations. Data are presented as mean ± SD. **d** Serum levels of IL-1β, IL-6, and TNFα in the LPS-induced endotoxemia model ($n = 3$ per group). Statistical analysis was performed using multiple t-tests: $^{*}p < 0.05$, $^{**}p < 0.01$, $^{***}p < 0.001$. Data are presented as mean ± SD.Statistical analysis was performed using Kaplan-Meier analysis with two-sided log-rank test for (**a**), two-sided multiple t-tests for (**c**, **d**). $^{*}p < 0.05$, $^{**}p < 0.01$, $^{***}p < 0.001$, $^{****}p < 0.0001$.Source data are provided as a Source Data file.

challenged THP-1 macrophages displayed elevated levels of IL-6, IL-1α, IL-1β, and TNF-α, all of which were significantly reduced by hCitH3-mAb (Fig. 6e). These results suggest that *P. aeruginosa* infection promotes CitH3 expression and secretion into BALF, and that hCitH3-mAb mitigates the pro-inflammatory activity of CitH3.

Parallel experiments with bone marrow–derived macrophages (BMDMs) from C57BL6 mice confirmed similar protective effects of hCitH3-mAb against BALF-induced injury and inflammation. In BMDMs, BALF derived from *P. aeruginosa*-septic mice activated pyroptosis markers, such as caspase-1 and cleaved gasdermin D (GSDMD) (Fig. 6f). Treatment with hCitH3-mAb reduced pyroptotic death by decreasing caspase-1 activation and GSDMD cleavage. Additionally, hCitH3-mAb significantly lowered the levels of IL-1α, IL-1β, IL-18, and LDH in the supernatant (Fig. 6g). These findings highlight the antibody's potential to modulate excessive inflammation and pyroptosis, a promising approach for managing sepsis-induced immune dysregulation.

Circulating CitH3 acts through TLR2 to trigger Ca^{2+}-dependent PAD2 auto-citrullination and its nuclear translocation

Previous studies from our team have demonstrated that systemic administration of CitH3 peptide induces systemic inflammation and pulmonary injury in mice[41]. Elevated CitH3 are thought to exacerbate NETosis and pyroptosis in neutrophils and macrophages, creating a vicious cycle of sustained cytokine production and tissue damage associated with ALI[40,41,49–51]. After establishing the efficacy of hCitH3-mAb in neutralizing CitH3-driven pathology, we turned to dissect the molecular mechanisms underpinning its function. To explore the autocrine role of CitH3 in macrophages, we tested its interaction with TLR2 receptors.

https://doi.org/10.1038/s41467-025-62788-6

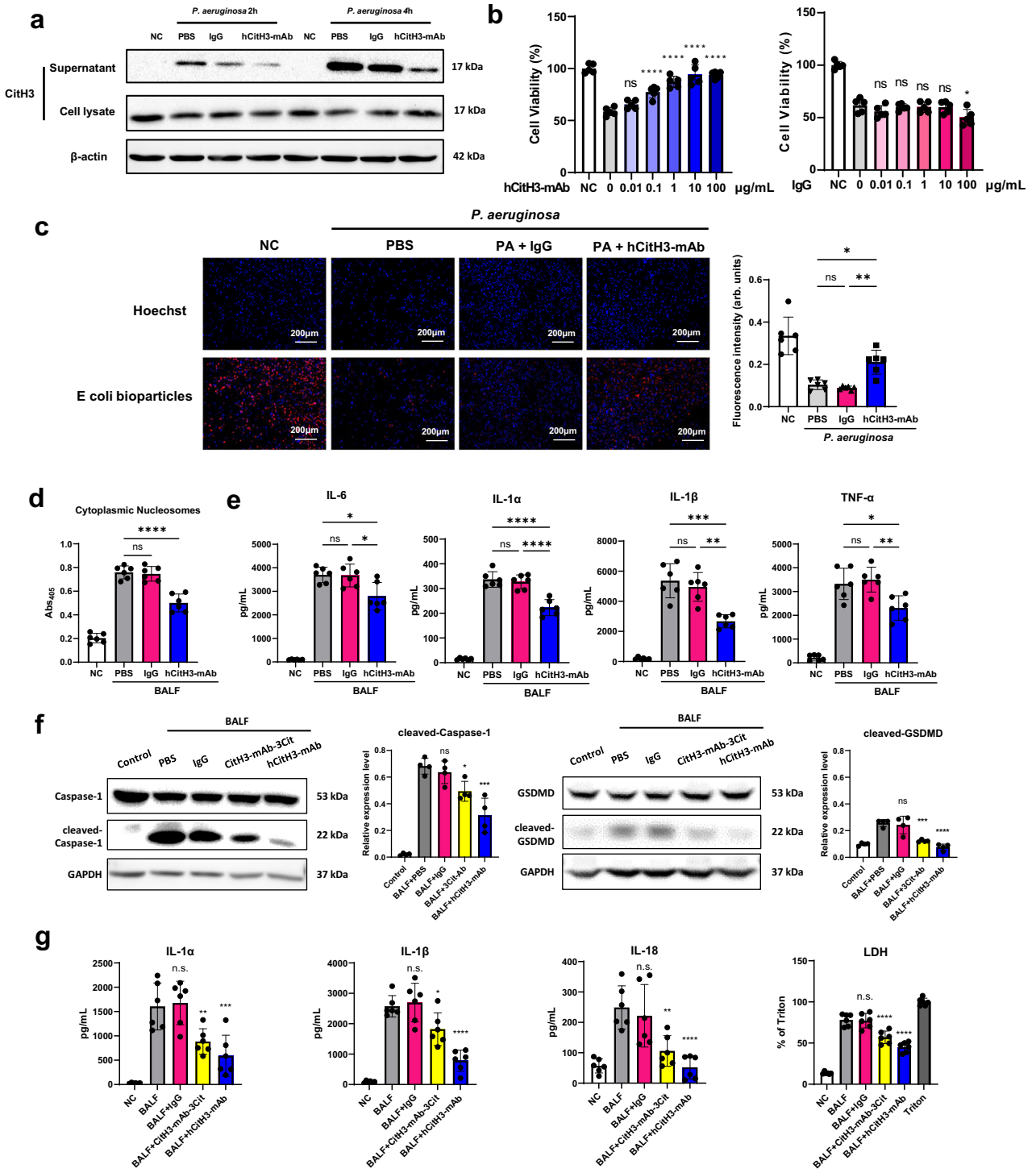

Immunocytochemistry revealed that Alexa Fluor 488-labeled CitH3 (CitH3-488) is efficiently taken up by BMDMs from wild-type (WT) mice within 5 min of incubation (Fig. 7a). In contrast, TLR2-deficient ($Tlr2^{-/-}$) BMDMs showed markedly reduced CitH3 uptake, implicating TLR2 in this process. Supernatant analysis of CitH3-treated BMDMs confirmed robust cytokine release (IL-1β, IL-6, TNF-α, TNF-β, and INF-β) in WT cells, whereas cytokine levels were significantly reduced in $Tlr2^{-/-}$ BMDMs (Fig. 7b). A non-citrullinated H3 peptide was used as a negative control, and LPS served as a positive control. The data demonstrate that CitH3, but not the unmodified H3 peptide, induces a cytokine response, while LPS acts as a potent inducer as expected. These controls underscore the specificity and biological relevance of CitH3-mediated cytokine induction.

To investigate whether CitH3 internalization is involved in PAD2 translocation, we examined the colocalization of CitH3 with Rab5, a well-established marker for early endosomes. As shown in Supplementary Fig. 5a, fluorescently labeled CitH3 colocalizes with Rab5, supporting its uptake via endosomal trafficking. To further probe the mechanism, we treated cells with Cytochalasin D, an inhibitor of actin polymerization that blocks endocytosis, and Dynasore, a dynamin inhibitor that blocks clathrin-mediated endocytosis. Both inhibitors markedly reduced CitH3 internalization (Supplementary Fig. 5b),

Fig. 6 | Bacteria-induced injury to macrophages is mitigated by hCitH3-mAb. **a** Immunoblot analysis of CitH3 levels in the supernatant (s.n.) and cell pellets of THP-1 cells pre-treated with hCitH3-mAb or human IgG (1.5 μg/mL), followed by exposure to *P. aeruginosa* (MOI 100) for 2 or 4 h. Similar results from three independent replicates. **b** Viability of THP-1 cells treated with *P. aeruginosa* at MOI 100 for 2 h with increasing doses of hCitH3-mAb or IgG ($n = 5$). **c** Phagocytic ability of THP-1 macrophage cells treated with hCitH3-mAb or human IgG (1.5 μg/mL) for 2 h, followed by *P. aeruginosa* exposure (MOI 100, 1 h) and incubation with pHrodo Red E. coli BioParticles (0.1 mg/mL). In representative images, red fluorescence indicates phagocytic activity, and blue signals represent Hoechst-stained nuclei. Fluorescence was measured at 560/585 nm ($n = 6$ biological replicates). Statistical analysis was performed using one-way ANOVA with Tukey's multiple comparisons test. **d** Cell death in THP-1 macrophages incubated with BALF for 4 h. BALF was collected from *P. aeruginosa*-induced septic mice pre-treated with either hCitH3-mAb (20 mg/kg) or human IgG (20 mg/kg) ($n = 6$ per group). BALF was collected in RPMI 1640 medium and filtered through a 0.22 μm filter. BALF was added at 12.5% of the final culture volume. **e** Levels of IL-6, IL-1α, IL-1β, and TNFα in the supernatant of THP-1 macrophages ($n = 6$ biological replicates) infected with *P. aeruginosa* (MOI 100, 2 h). NC indicates the negative control group. BALF was added at 12.5% of the final culture volume. **f** Western blot analysis of pyroptosis markers, including Caspase-1 and GSDMD cleavage products, in BMDMs treated with BALF as described in (**e**). hCitH3-mAb treatment was more effective than the commercial CitH3-mAb-3Cit in mitigating BALF-induced pyroptosis in BMDMs ($n = 4$ biological replicates). Human IgG was used as negative control. **g** Levels of IL-1α, IL-1β, IL-18, and LDH in the supernatant of BMDM cells treated with BALF. hCitH3-mAb demonstrated greater efficacy than commercial CitH3-mAb-3Cit in reducing BALF-induced pro-inflammatory cytokine release in BMDMs ($n = 6$ biological replicates).Data are presented as mean ± SD. Statistical analyses were conducted using one-way ANOVA and Dunnett's test, with comparisons among the BALF-treated group for (**d**–**g**), and to the '0' group for (**a**, **b**): $^{*}p < 0.05$, $^{**}p < 0.01$, $^{***}p < 0.001$, $^{****}p < 0.0001$.Source data are provided as a Source Data file.

indicating that active endocytic processes are involved. These findings support a role for endocytosis in CitH3 uptake into BMDMs.

Confocal microscopy showed that CitH3 rather than H3 treatment altered PAD2's subcellular localization, promoting its translocation from the cytoplasm to the nucleus, where it co-localized with DAPI-stained nuclear regions (Fig. 7c, Supplementary Movies. 1-4). Subcellular fractionation further confirmed this nuclear translocation of PAD2 following CitH3 exposure (Fig. 7d). Notably, CitH3-induced nuclear translocation appeared to have more pronounced effect on PAD2 compared to PAD4, which predominantly resides in the nucleus under basal conditions (Supplementary Fig. 6).

Immunoblot analysis revealed that PAD2 undergoes auto-citrullination in the nuclear fraction after CitH3 treatment, suggesting this as a potential mechanism of activation (Fig. 7e). Ca^{2+} imaging of WT BMDMs demonstrated a significant increase in intracellular Ca^{2+} within 5 min of CitH3 treatment, an effect absent with non-citrullinated H3 (see Supplementary Fig. 7). This CitH3-induced Ca^{2+} elevation was dependent on extracellular Ca^{2+}, as removal of extracellular Ca^{2+} abolished the response.

Using our established in vitro citrullination assay[52,53], we confirmed PAD2's ability to catalyze H3 citrullination in a Ca^{2+}-dependent manner. Briefly, recombinant human histone H3 was incubated with MBP-tagged recombinant human PAD2 in a reaction buffer or a Ca^{2+}-free reaction buffer containing EGTA for Ca^{2+} chelation at 37 °C for 4 h. Citrullinated proteins were then captured by citrulline-specific biotin-probe and further captured using streptavidin-agarose beads. As analyzed by western blotting, EGTA-mediated Ca^{2+} chelation significantly reduced CitH3 production (Fig. 7e). Interestingly, the PAD2 enzyme used in these assays exhibited auto-citrullination, which diminished with EGTA in the reaction buffer.

To investigate PAD2 auto-citrullination further, we performed biochemical assays using MBP-PAD2 and His-PAD2 in the same reaction buffer, testing their capacity for cross-citrullination (Fig. 7f). Indeed, strong cross-citrullination was observed between MBP-PAD2 and His-PAD2 in the presence of Ca^{2+}, an effect significantly reduced by EGTA chelation of Ca^{+2}. Interestingly, when PAD4 was included in the reaction buffer, we observed an added effect of PAD4 and PAD2 in facilitating citrullination of both His-PAD2 and MBP-PAD2.

These findings suggest a mechanistic pathway whereby circulating CitH3, acting through TLR2, triggers intracellular Ca^{2+} elevation and activates PAD2. This leads to PAD2 auto-citrullination and nuclear translocation, thereby amplifying CitH3 production and exacerbating NETosis, perpetuating the vicious cycle of CitH3-mediated inflammation observed in sepsis and ALI. Importantly, this mechanism highlights the therapeutic advantage of hCitH3-mAb: unlike many commercial antibodies that primarily recognize PAD4-mediated CitH3 (R2, R8, R17), hCitH3-mAb is capable of neutralizing CitH3 generated by both PAD2 and PAD4. This broader recognition profile enables hCitH3-mAb to effectively disrupt the CitH3 amplification loop regardless of its enzymatic origin, making it a uniquely potent candidate for intervening in sepsis-related inflammation.

hCitH3-mAb mitigates CitH3-mediated cytokine storm in macrophages

Having uncovered a CitH3–TLR2–PAD2 feedback loop that amplifies inflammation and cellular injury, we next sought to determine how hCitH3-mAb might therapeutically intervene in this process. Specifically, we investigated whether hCitH3-mAb could protect macrophages from CitH3-induced damage and thereby support their function under septic conditions.

To this end, we assessed the effects of CitH3 on macrophage viability. BMDMs exposed to increasing doses of CitH3 peptide showed dose-dependent injury, as indicated by elevated LDH release (Fig. 8a) and reduced cell viability measured by CCK-8 assay (Fig. 8b). By contrast, the unmodified H3 peptide had no effect on BMDM viability. Remarkably, escalating doses of hCitH3-mAb provided dose-dependent protection against CitH3-induced injury, a benefit not observed with control human IgG (Fig. 8c, d).

Western blot analysis revealed a time-dependent release of CitH3 protein (17 kD) from BMDMs upon exposure to exogenous 30-amino acid CitH3 peptide (Fig. 8e), indicating that extracellular CitH3 can initiate a self-amplifying inflammatory and injurious response in macrophages. Further quantification of citrullinated proteins in BMDM lysates showed a marked increase in citrullination after just one hour of CitH3 peptide treatment (Supplementary Fig. 9). To determine whether PAD activation was essential for CitH3-mediated citrullination, we assessed BMDMs from Pad2 knockout (*Pad2*−/−) and Pad2/4 double knockout (*Pad2*−/−*Pad4*−/−) mice. While CitH3 treatment elevated CitH3 protein levels and total citrullinated proteins in WT BMDMs, no such increased was observed in *Pad2*−/− or *Pad2*−/−*Pad4*−/− cells (Fig. 8f).

These results reinforce the hypothesis that CitH3 activates Ca^{2+}-dependent PAD enzymes, which drives increased citrullination of H3 and PAD2, perpetuating a self-sustained cycle of CitH3 production. To determine whether hCitH3-mAb could interrupt this cycle, BMDMs were treated with varying doses of hCitH3-mAb in the presence of CitH3 peptide (Fig. 8g). hCitH3-mAb treatment significantly reduced CitH3-induced pro-inflammatory cytokines, including IL-6, IL-1β, and TNF-α, as well as interferons IFN-α and IFN-β, indicating decreased TLR2 activation.

In parallel studies using bone marrow-derived neutrophils (BMDNs), we observed that treatment with CitH3 peptide induced a time-dependent release of double-stranded DNA (dsDNA), a key biomarker for NETosis (Supplementary Fig. 10a). Notably, incubation with hCitH3-mAb significantly reduced NETosis, as evidenced by the

https://doi.org/10.1038/s41467-025-62788-6

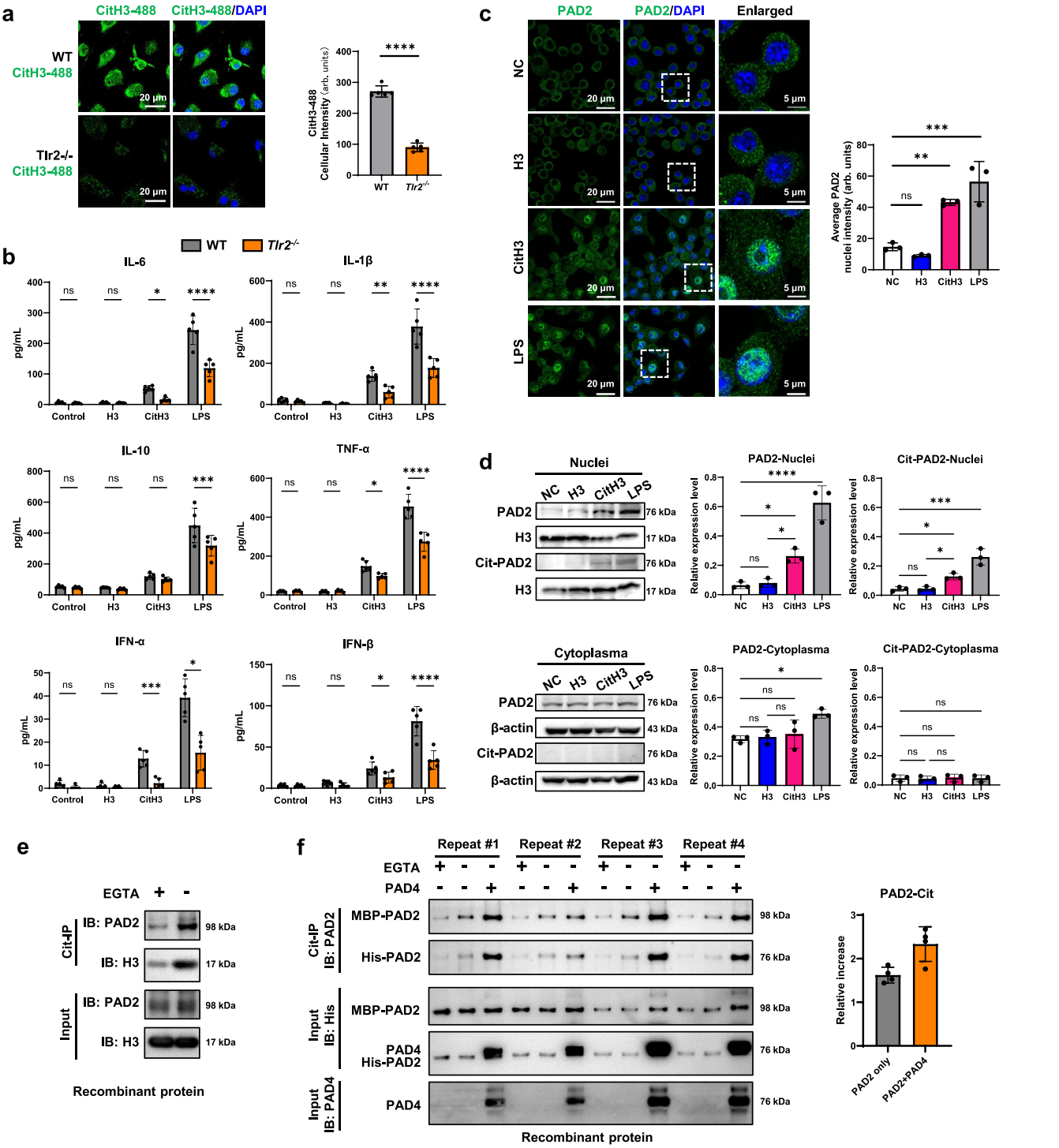

decreased levels of dsDNA (Supplementary Fig. 10a). Our hCitH3-mAb demonstrated superior efficacy in mitigating CitH3-induced NETosis compared to a commercially available CitH3-mAb-3Cit (Supplementary Fig. 10b). As a control, treatment with human IgG showed no effect on CitH3-induced dsDNA release from BMDNs. Consistently, CitH3 peptide induced NETs formation, as indicated by co-localization of CitH3 and MPO with DNA; hCitH3-mAb significantly attenuated NETosis, whereas hIgG had no effect (Supplementary Fig. 10c).

Together, these results demonstrate that hCitH3-mAb effectively disrupts the CitH3-TLR2-PAD2 pathway, providing a compelling basis for its use as a therapeutic strategy to mitigate the inflammatory cascade and cytokine storm in sepsis.

Discussion

Our study provides a comprehensive evaluation of a novel humanized monoclonal antibody targeting citrullinated histone H3 (hCitH3-mAb) for therapeutic intervention in sepsis - a condition marked by severe immune dysregulation and multi-organ injury. This fully humanized antibody effectively neutralizes tissue damage associated with NETosis without impairing the antimicrobial functions of neutrophil extracellular traps (NETs), offering a targeted therapeutic strategy that overcomes the limitations of prior non-specific anti-PAD approaches, which often led to unintended immunosuppression. By neutralizing CitH3, a key driver of excessive NETosis and pyroptosis, hCitH3-mAb reduces proinflammatory cytokine production, restores immune cell

Fig. 7 | Circulating CitH3 triggers Ca^{2+}-dependent PAD2 auto-citrullination and nuclear translocation via TLR2 signaling. a Immunofluorescence analysis showing efficient uptake of Alexa Fluor 488-labeled CitH3 (5 μg/mL) by wild-type (WT) BMDMs but not by $Tlr2^{-/-}$ BMDMs. Cellular intensity of Alexa-488 was quantified ($n = 5$). Statistical analysis was performed using two-sided, Unpaired t test with Welch's correction. **b** Cytokine profiling of pro- and anti-inflammatory mediators (IL-6, IL-1β, IL-10, TNFα, IFN-α, IFN-β) in supernatants of WT and $Tlr2^{-/-}$ BMDMs treated with H3 or CitH3 peptides (15 μg/mL) for 16 h (n = per group). LPS (200 ng/mL) served as positive control. Statistical analysis was performed using two-way ANOVA with Sidak's multiple comparisons test. **c** Immunocytochemistry demonstrating nuclear translocation of PAD2 in BMDMs after 1 h exposure to CitH3 peptide (15 μg/mL). LPS (200 ng/mL) served as a positive control. PAD2 was stained with Alexa Fluor 488 (green), and nuclei were counterstained with DAPI (blue). Quantification of PAD2 nuclear localization was analyzed by one-way ANOVA followed by Tukey's multiple comparisons test ($n = 3$ per group). **d** Subcellular fractionation analysis confirming significant nuclear localization and citrullination of PAD2 in WT BMDMs following treatment with H3, CitH3, or LPS. Quantification was analyzed using one-way ANOVA followed by Tukey's multiple comparisons test (n = per group). **e** In vitro citrullination assay showing MPB-tagged PAD2-mediated citrullination of H3 in a Ca^{2+}-dependent manner. EGTA-mediated Ca^{2+} chelation eliminated CitH3 production. Similar results from three independent replicates. **f** In vitro citrullination assay showing PAD2 citrullination. PAD2 auto-citrullination was confirmed as His-tagged recombinant PAD2 co-incubated with MBP-tagged PAD2 resulted in PAD2 citrullination. PAD4 also promotes PAD2 citrullination. Quantification was performed by Image J, citrullination signals were normalized to corresponding input signals and further normalized to the matching EGTA-treated group in each replicate experiments. Statistical analysis was performed using two-sided t-test.Data are presented as mean ± SD. Statistical significance in all panels was determined as follows: $^{*}p < 0.05$, $^{**}p < 0.01$, $^{***}p < 0.001$, $^{****}p < 0.0001$. Source data are provided as a Source Data file.

function, and significantly improves survival in murine models of sepsis. In addition to neutrophils, we identify macrophages as a previously unrecognized but substantial source of CitH3, providing a cell-specific perspective on CitH3 regulation with important implications for innate immunity and sepsis pathogenesis. We also describe a previously unreported positive-feedback mechanism in which PAD2 undergoes auto-citrullination, leading to sustained CitH3 production. Mechanistically, we uncover a CitH3–TLR2–PAD2 feedback loop that amplifies inflammation and tissue damage by promoting PAD2 activation and persistent CitH3 expression. Importantly, hCitH3-mAb disrupts this pathological cycle, curbing immune overactivation while preserving the physiological functions of NETs - offering a safe and effective strategy for treating sepsis and related immune dysregulation disorders.

A notable advantage of hCitH3-mAb over existing commercial CitH3 antibodies lies in its ability to bind CitH3 residues generated by both PAD2 and PAD4 enzymes[40] (Figs. 2 and 3). Commercial antibodies are limited to targeting PAD4-mediated citrullinated residues (typically at R2, R8, and R17), which represent only a subset of CitH3 modifications. In contrast, hCitH3-mAb's broader epitope recognition enables more effective neutralization of CitH3, regardless of its enzymatic origin. This expanded specificity allows it to neutralize CitH3 more effectively, thereby reducing inflammation and improving survival in murine models. These findings underscore the therapeutic potential of targeting PAD2, a critical enzyme in CitH3 biogenesis, which has been implicated in sepsis pathology but remains underexplored in therapeutic research[37,54].

Beyond its therapeutic application, hCitH3-mAb also demonstrates utility as a diagnostic and monitoring tool. Building on prior research[46–48], we utilized the PEdELISA platform to precisely quantify CitH3 levels as a biomarker of sepsis onset and progression (Fig. 3 and Supplementary Fig. 3). PEdELISA offers significant advantages over traditional ELISA, including faster processing, higher sensitivity, and the ability to work with small sample volumes. Using hCitH3-mAb in the PEdELISA platform, we demonstrated that CitH3 levels increased in sepsis non-survivors but declined in sepsis survivors. In contrast, serum CitH3 levels in non-infectious ALI patients were indistinguishable from those in healthy individuals. These findings reinforce the diagnostic potential of hCitH3-mAb and the utility of PEdELISA for identifying critical therapeutic windows, supporting real-time monitoring of inflammatory responses in clinical settings.

Our in vivo studies utilized a *Pseudomonas aeruginosa* strain (ATCC 19660), previously reported by other groups to induce pyroptosis in lung epithelial cells and immune tissues, further validating its relevance as a model for studying inflammatory cell death in the context of infection-induced sepsis[55–60]. We demonstrated that hCitH3-mAb effectively protects macrophages from injury induced by both *P. aeruginosa* and CitH3. In vivo, hCitH3-mAb treatment preserved macrophage viability, reduced expression of pyroptosis markers, and maintained phagocytic function despite ongoing bacterial infection and inflammatory stress. Additionally, hCitH3-mAb reduced excessive NETosis, thereby preserving neutrophil function and preventing their premature depletion. This combined stabilization of macrophage and neutrophil activity likely contributes to the reduced bacterial burden observed in hCitH3-mAb–treated mice, underscoring the antibody's dual benefit in controlling infection and mitigating immune overactivation. While pyroptosis and NETosis are clearly implicated, other forms of regulated cell death—such as apoptosis and necroptosis—may also play a role. Further studies are needed to fully elucidate the mechanisms by which hCitH3-mAb protects immune cells under inflammatory stress and to define its broader immunomodulatory potential.

Our study elucidates the CitH3-TLR2-Ca^{2+}-PADs pathway, offering valuable insights into the mechanisms underlying CitH3 self-amplification. Mechanistic investigations revealed that CitH3 activates the TLR2 signaling pathway, triggering intracellular calcium elevation, PAD2 auto-citrullination, and subsequent nuclear translocation. To determine whether CitH3 internalization contributes to PAD2 activation, we examined its colocalization with Rab5, an early marker of endosomes and phagosomes. CitH3 colocalized with Rab5, suggesting uptake via vesicular trafficking. Inhibiting phagocytosis with cytochalasin D or endocytosis with Dynasore significantly reduced CitH3 internalization, confirming the role of active vesicular transport in CitH3 uptake by BMDMs and its downstream activation of NETosis. This observation is consistent with previous studies demonstrating that activated TLR2 facilitates the uptake of molecules via endosomes[61–63], aligning with the observed slower CitH3 uptake in $Tlr2^{-/-}$ cells. Calcium imaging demonstrated that CitH3 induces intracellular calcium elevation within five minutes, a response that is absent with unmodified H3. TLR2 activation is also known to stimulate calcium flux in various cell types, as supported by previous studies[64–66]. Importantly, $Tlr2^{-/-}$ cells fail to exhibit calcium flux or pro-inflammatory signaling[67], underscoring TLR2's critical role in this pathway. Our findings demonstrate that PADs, in conjunction with Ca^{2+}, facilitates PAD2 auto-citrullination and nuclear translocation, forming the foundation of a self-sustaining CitH3 production and inflammatory feedback loop. Crucially, hCitH3-mAb disrupts this loop by neutralizing extracellular CitH3, thereby reducing TLR2 activation, dampening downstream inflammatory signaling, and preserving macrophage and neutrophil function. All together, these findings illuminate the molecular underpinnings of CitH3-mediated inflammation and highlight pivotal therapeutic intervention points to counteract its effects.

Despite these promising results, several limitations warrant consideration. First, while murine models provide valuable insights, they do not fully replicate the complexity and heterogeneity of human sepsis. Validation in large animal models is essential to confirm the safety, efficacy, and translational potential of hCitH3-mAb under

https://doi.org/10.1038/s41467-025-62788-6

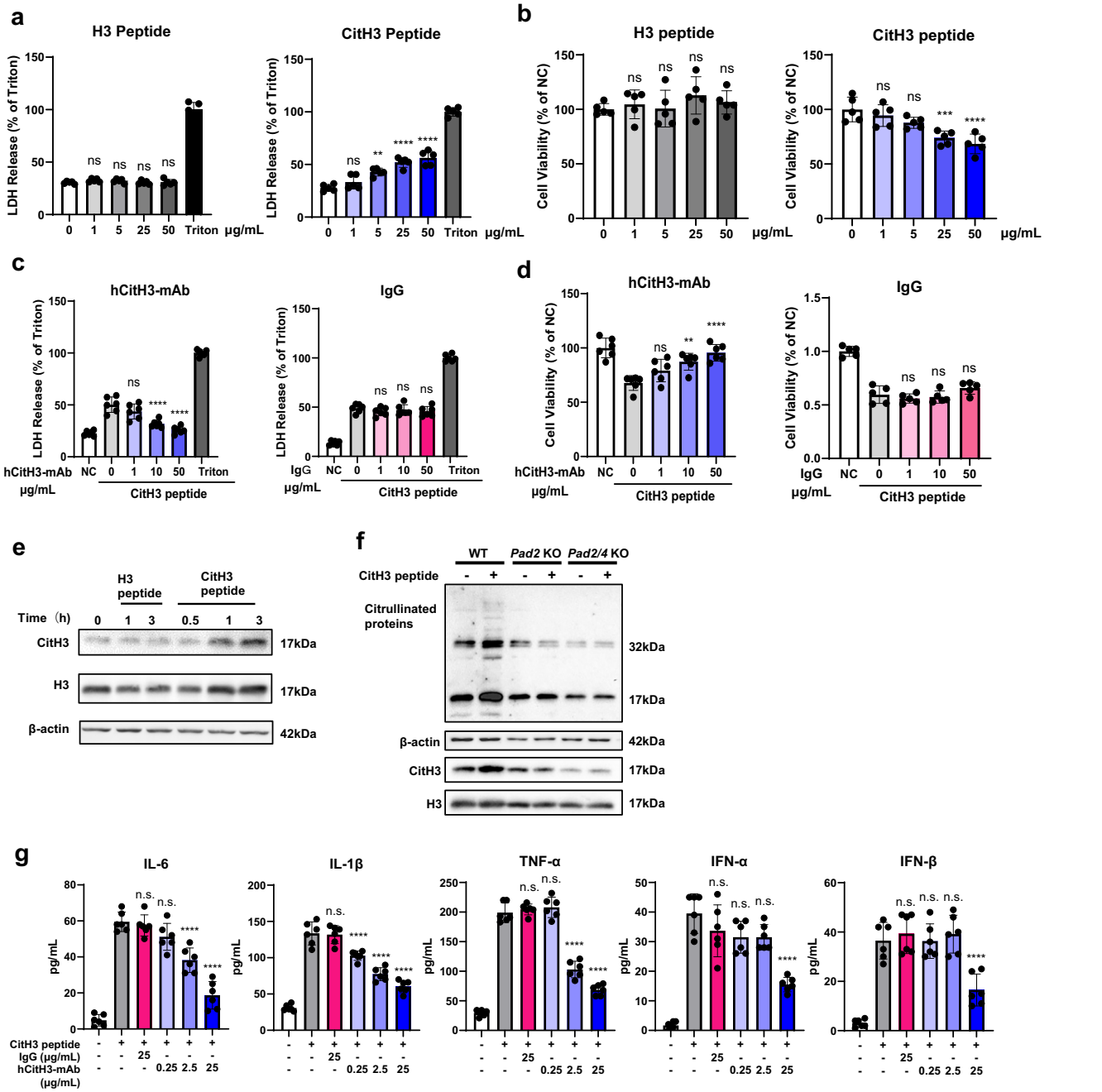

Fig. 8 | hCitH3-mAb preserves macrophage integrity and mitigates CitH3-induced cytokine storm. a LDH release from supernatants of BMDMs treated with increasing doses of CitH3 or unmodified H3 peptides for 24 h at 37 °C, showing CitH3-induced cytotoxicity (n = per group). **b** Cell viability, assessed using the CCK8 assay, demonstrated significant reduction following CitH3 peptide treatment compared to the H3 peptide ($n = 5$ per group). **c** BMDMs treated with 50 μg/mL CitH3 peptide and increasing doses of hCitH3-mAb or human IgG. LDH release was measured to evaluate cytotoxicity (n = per group).**d**, Viability of BMDMs treated as in (**c**) was measured using the CCK8 assay. hCitH3-mAb significantly preserved cell viability compared to control IgG (n = per group). **e** Immunoblot analysis of CitH3 in BMDMs treated with 15 μg/mL CitH3 or H3 peptides. Cells were washed three times prior to collection. And given that the CitH3 peptide is only ~30 amino acids in length, the bands observed at ~17 kDa are interpreted as endogenous cellular CitH3 protein detected at various time points. Similar results from three independent replicates. **f** Western blot analysis of citrullinated proteins in BMDMs from WT, Pad2$^{-/-}$, and Pad2/4$^{-/-}$ mice following 1 h treatment with 15 μg/mL CitH3 peptide. CitH3-induced citrullination was PAD2-dependent. Similar results from four independent replicates. **g** Quantification of IL-6, IL-1β, TNFα, IFN-α, and IFN-β levels in the supernatants of BMDMs treated with 25 μg/mL CitH3 peptide for 24 h ($n = 6$ per group). hCitH3-mAb effectively reduced CitH3-induced cytokine elevation in a dose-dependent manner, whereas control IgG had no effect. Data are presented as mean ± SD. Statistical analysis: One-way ANOVA followed by Dunnett's multiple comparisons test was applied throughout. Comparisons were made to the '0' group in (**a**–**d**), and the CitH3-treated group in (**g**), as indicated. Significance thresholds: $^{*}p < 0.05$, $^{**}p < 0.01$, $^{***}p < 0.001$, $^{****}p < 0.0001$.Source data are provided as a Source Data file.

clinically relevant conditions. Second, while our data support endocytosis-mediated uptake of CitH3 and its contribution to intracellular NETosis activation, we cannot rule out the possibility that membrane-delimited signaling via CitH3–TLR2 interactions at the plasma membrane also contributes to PAD2 activation. Understanding how CitH3 is released into the extracellular environment is also critical for explaining its pathological accumulation during sepsis. CitH3 release likely involves both passive and active mechanisms, depending on the context and immune cell activation state[68,69]. While passive release through lytic NETosis and pyroptosis is well established, the possibility of active secretion from viable cells remains an intriguing area that warrants further investigation. Third, our PEdELISA studies were conducted on a limited number of samples. Larger cohorts are necessary to further validate PEdELISA's reliability and utility as a diagnostic and monitoring tool in clinical settings. Fourth, our study primarily focused on acute sepsis and did not investigate chronic conditions. Exploring the long-term effects of hCitH3-mAb treatment across a broader spectrum of diseases will provide a more comprehensive understanding of its therapeutic potential and clinical applicability. Finally, beyond the CitH3-induced inflammatory cycle, other citrullinated proteins may act as autoantigens, leading to the production of anti-citrullinated protein antibodies (ACPA), which are biomarkers for autoimmune diseases like rheumatoid arthritis[70,71]. The role of these citrullinated proteins in sepsis and their contribution to immune dysregulation remain to be elucidated.

Looking ahead, our future efforts will focus on translating these findings into clinical applications. This will involve advancing hCitH3-mAb through extensive preclinical studies, including chemistry, manufacturing, and controls (CMC) to ensure scalable and consistent production in GMP facilities, GLP-compliant toxicology evaluations, and the development of robust clinical protocols to secure FDA approval for an Investigational New Drug (IND) application. Additionally, exploring combination therapies with hCitH3-mAb and complementary anti-inflammatory or antimicrobial agents could further enhance its therapeutic efficacy.

In summary, hCitH3-mAb represents a promising therapeutic candidate for addressing the critical unmet clinical needs, particularly in sepsis treatment. By targeting a critical mediator of immune dysregulation, hCitH3-mAb offers a novel approach to mitigating inflammation, preventing cytokine storms, and reducing organ injury. While its primary focus is on addressing the urgent clinical challenges of sepsis, its therapeutic potential extends to a broader spectrum of immune-driven conditions, including acute respiratory distress syndrome (ARDS), disseminated intravascular coagulation (DIC)/thrombosis, autoimmune diseases, and ischemia-reperfusion injury, highlighting its versatility and transformative potential in combating life-threatening inflammatory diseases.

Methods

Ethics statement

This study involving human participants was reviewed and approved by the University of Michigan and the University of Mississippi Medical Center institutional review boards (IRB; HUM00056630 and IRB#201-0261, respectively). The study was conducted following the principles of the Declaration of Helsinki and in accordance with US Federal Policy for the Protection of Human Subjects. All participants or their legal proxy signed informed consent for the parent study which included permission to store and use remaining blood samples indefinitely under a University of Michigan IRB approved secondary analysis protocol (HUM00150839). All animal studies were conducted in compliance with institutional and national guidelines for the care and use of laboratory animals. The study protocols were reviewed and approved by the Institutional Animal Care and Use Committee (IACUC) at University of Michigan (PRO00011567). All efforts were made to minimize animal suffering and reduce the number of animals used in the experiments. All data supporting the findings of this study are available within the paper and its Supplementary Information.

Generation of hCitH3-mAb

Cryopreserved hybridoma cells secreting mouse CitH3-mAb24[40] were cultured in RPMI-1640 medium supplemented with 10–20% ultra-low IgG fetal bovine serum (Gibco). Total RNA was extracted using the Qiagen RNeasy Kit and reverse-transcribed to complementary DNA (cDNA) using the GE Life Sciences First Strand cDNA Synthesis Kit. cDNA sequences were determined by ProMab Biotechnologies, Inc. (Richmond, CA). Humanization and optimization of the mouse CitH3-mAb to generate humanized CitH3-mAb (hCitH3-mAb) were conducted by Ab Studio, Inc. (Hayward, CA), a biotechnology company specializing in AI-based antibody engineering.

For expression, Bon Opus Biosciences (Millburn, NJ) designed and optimized vectors encoding diverse VH and VL chain combinations. These vectors were transfected into CHO cells to maximize binding activity and yield. Rigorous quality control was conducted iteratively to ensure high-yield, high-purity production. Thermal stability tests, including RF-HPLC chromatography, confirmed batch production consistency and absence of aggregation (see flow chart outlined in Fig. 1a). SparX Biopharmaceutical Corp. (Mount Prospect, IL), a CDMO specializing in clinical-grade antibody production, performed developability studies. This included optimization of upstream and downstream processes to ensure scalable production and purification of GMP-grade hCitH3-mAb. Stable CHO-GS KO cell lines with high-titer expression of hCitH3-mAb were established and used for production of the final product, which was subsequently validated for preclinical studies. The sequence of the CH1–CH3 domain indicates that it is of the IgG1 subtype; therefore, we use IgG1 (Biolegend, 403501) as the isotype negative control. The sequence is as follows:

ASTKGPSVF-
PLAPSSKSTSGGTAALGCLVKDYFPEPVTVSWNSGALTSGVHTFPAVLQSS
GLYSLSSVVTVPSSSLGTQTYICNVNHKPSNTKVDKKVEPKSCDKTHTCPP
CPAPELLGGPSVFLFPPKPKDTLMISRTPEVTCVVVDVSHEDPEVKFNWYV
DGVEVHNAKTKPREEQYNSTYRVVSVLTVLHQDWLNGKEYKCKVSNKA
LPAPIEKTISKAKGQPREPQVYTLPPSREEMTKNQVSLTCLVKGFYPSDIAV
EWESNGQPENNYKTTPPVLDSDGSFFLYSKLTVDKSRWQQGNVFSCSVM
HEALHNHYTQKSLSLSPGK

Synthesis of CitH3 and H3 peptides

The CitH3 and H3 peptides were synthesized by Chinese Peptide Company Ltd. (Zhejiang, China). The peptide sequence of H3 is "H2N-ARTKQTARKSTGGKAPRKQLATKAARKSAPC-amide", and CitH3 is "H2N-A(Cit)TKQTA(Cit)KSTGGKAP(Cit)KQLATKAA(Cit)KSAPC-amide". They were both of high purity ≥95% determined by HPLC.

Human samples

Serum samples and clinical data were obtained from patients with or without sepsis[31], enrolled in an observational study at the University of Michigan and the University of Mississippi Medical Center. Sample preparation and patient information collection have been previously detailed[31].

Septic shock patients were adults (≥18 years) who presented to the emergency department and met the consensus definitions for septic shock at the time of enrollment: confirmed or suspected infection, at least two systemic inflammatory response criteria, and evidence of hypoperfusion (systolic blood pressure <90 mmHg after fluid resuscitation or blood lactate ≥36 mg/dL). Non-infectious controls were ED patients who presented with shock—defined as the need for vasopressors or persistent hypotension (SBP < 90 mmHg or MAP < 65 mmHg) after receiving at least 2 L of fluid—but without any clinical or laboratory evidence of infection.

Animal models of sepsis

C57BL/6 J, B6.129-Tlr2tm1Kir/J, B6(Cg)-Tlr4tm1.2Karp/J mice, aged between 8 and 12 weeks, were obtained from the Jackson Laboratory (Bar Harbor, ME, USA) and housed in a specific pathogen-free facility under controlled environmental conditions. All experimental procedures were conducted following the guidelines set forth by the University of Michigan and University of Virginia Institutional Animal Care and Use Committee, ensuring strict adherence to approved protocols for ethical animal research.

Pseudomonas aeruginosa (Schroeter) Migula (ATCC) 19660 was used for infection experiments. In the *Pseudomonas aeruginosa* (*P. aeruginosa*) infection model, mice were lightly anesthetized and 2.5×10^6 colony-forming units (CFU) of *P. aeruginosa* was administered as a 30 μL intranasal drop to ensure uniform exposure to the respiratory tract. Animals were randomized with different treatment. For the lipopolysaccharide (LPS)-induced endotoxemia model, LPS was dissolved in sterile saline (5 mg/mL) and administered via intraperitoneal injection at a dose of 25 mg/kg. Treatment groups received either hCitH3-mAb antibody (20 mg/kg) or an equivalent dose of human IgG (Sigma) at a final volume of 200 uL, both administered via tail vein injection. To assess survival, mice were monitored for more than 10 days post-infection or until the experiment's conclusion, with survival data recorded daily by a blinded investigator. Humane endpoints were strictly observed to minimize animal suffering. The dose and sample size were based on previous study[39–41]. For fine-time monitoring, blood samples were collected from the tail vein at specified time points for systemic marker analysis. Tissues and organs were harvested 24 h post-infection for histological and molecular evaluations. All experiments adhered to institutional guidelines and approved protocols for animal research to ensure ethical treatment and minimizing suffering throughout the study.

Bacterial clearance

The bacterial burden in different organs was quantified by homogenizing the tissues. After homogenization, tissue samples were serially diluted in sterile saline, and aliquots were spread onto agar plates. The plates were incubated at 37 °C for 16 h to allow bacterial colony growth. Colonies were counted using ImageJ software, and the colony-forming units (CFUs) per gram of tissue was calculated by a blinded investigator.

Hematoxylin and eosin staining

The severity of acute lung injury was evaluated through histopathological analysis of lung tissues. Lungs were fixed in paraffin wax, sectioned into 4 μm thick slices, and stained with hematoxylin and eosin (H&E) to evaluate tissue morphology. A blinded pathologist, unaware of the experimental groups, conducted assessment of the histological sections. The severity of lung injury was graded using Suzuki's scoring system on a scale from 0 to 5, where 0 represents no injury and 5 indicated the most severe injury[72]. The airspace proportion, defined as the ratio of the airspace area to the total area, was calculated to quantify structural damage. Lower airspace proportions indicated alveolar wall thickening, airspace loss, and impaired respiratory function.

Chip preparation and pre-equilibrium digital ELISA (PEdELISA)

The PEdELISA chip fabrication, surface functioning and detailed assay protocol was adapted from previously established methods[46]. Briefly, The PEdELISA chip is constructed using laser-cut PMMA layers and pressure-sensitive adhesives (PSA) to form a multilayer structure suitable for mass production. The top PMMA layer, interfacing with the fluidic manifold, is laser-cut to create inlet/outlet ports and alignment features. A PSA layer forms flow cells when laminated between the PMMA top layer and the bottom digital sensor chip. The bottom digital sensor comprises femtoliter-sized microwell arrays molded from polydimethylsiloxane (PDMS) onto a glass substrate. For microarray patterning, reusable PDMS flow cell direct analyte-specific beads (1 mg/mL) into microwells. After bead settling and washing with PBS-T, the top PMMA/PSA assembly is permanently bonded to the chip, creating 16 flow cells for multiplexed cytokine measurements. Flow cells are blocked with SuperBlock™ buffer to prevent non-specific binding. Bead-filling rates are verified microscopically, and completed chips are sealed and stored at 4 °C.

The PEdELISA assay workflow includes whole blood incubation, detection antibody labeling, streptavidin-HRP labeling, substrate loading, oil sealing, and fluorescence imaging. An automated engineering prototype of the PEdELISA system has been developed, enabling it to function as a stand-alone system at the point of care. This system comprises the PEdELISA chip, a 3D-printed fluidic manifold, a syringe pump with rotary valves, and a compact, custom-built fluorescence reader. Automated reagent handling requires 30–40 min, while imaging takes less than 5 min, resulting in a total operational assay time of approximately 1 h for up to 16 samples and 6-plex detection. Data analysis is performed using a custom-trained convolutional neural network (CNN)[48,73], which detects and counts fluorescence spots, identifies image dust and defects, evaluates the brightfield bead filling rate, and calculates the digital immunoassay signal as "Average Enzyme Molecule per Bead (AEB)."

Cell culture

Cells were cultured in a humidified atmosphere with 5% CO_2 at 37 °C. THP-1 cells were maintained in RPMI-1640 complete medium supplemented with 10% fetal bovine serum (FBS), 100 U/mL penicillin, and 100 μg/mL streptomycin. The cells were subcultured every 2–3 days to maintain cell viability and prevent overgrowth, and differentiated into macrophages using 100 ng/mL PMA (Sigma) for 48 h for experimentation with *P. aeruginosa*, BALF and CitH3.

Bone marrow cells were collected from femurs and tibias of mice. Bone marrow-derived macrophages (BMDMs) were generated by culturing bone marrow cells in macrophage differentiation medium for 7 days. The medium consisted of RPMI-1640 complete medium with 20 ng/mL CSF (Peprotech, AF-315-02). The differentiation medium was replaced every 2–3 days to ensure optimal cell growth and differentiation.

Mouse neutrophils were isolated from harvested bone marrow cells. After lysing red blood cells on ice for 10 min, the cells were resuspended in 1–3 ml of sterile PBS. A density gradient was prepared using 3 ml of Histopaque 1119 layered over 3 ml of Histopaque 1077 in a 15 ml conical tube. The bone marrow cell suspension was carefully layered on top and centrifuged at 872 × g for 30 min at room temperature without a brake. Neutrophils were collected at the interface of the Histopaque 1119 and 1077 layers, washed twice with RPMI 1640 medium, and then challenged with 500 nM phorbol myristate acetate (PMA) and incubated for 3 h at 37 °C.

Immunofluorescence assay

For general immunocytochemistry assays, cells were fixed with cold methanol for 5 min, permeabilized with 0.05% Triton X-100 in PBS for 10 min, and then blocked with 5% BSA. Cells were incubated with primary antibodies overnight at 4 °C, followed by fluorescently labeled secondary antibodies (Invitrogen, USA). Nuclei were counterstained with DAPI. Three gentle washes with PBS between each step.

For the cell uptake assay, CitH3 peptides were labeled with Alexa Fluor 488 dye (Thermo Fisher, 46403) according to the manufacturer's protocol. BMDMs were treated with 5 μg/mL of fluorescently labeled CitH3 peptide for 5 min, followed by three gentle washes with PBS to remove unbound peptide. To block specific internalization pathways, cells were pretreated with cytochalasin D (Sigma C8273, 10 μM, 1 h) to inhibit phagocytosis, or with Dynasore (Sigma D7693, 80 μM, 1 h) to inhibit endocytosis via dynamin-dependent endosome formation. Cells were then fixed with 4% paraformaldehyde for 10 min to preserve internalized material. After fixation, cells were permeabilized and

processed for immunocytochemistry using standard procedures, including incubation with primary and secondary antibodies as described above. The primary antibodies used in immunocytochemistry assays: PAD2 (12110-1-AP), PAD4 (17373-1-AP), Rab5 (CST, 3547), EEA1 (CST, 3288), MPO (Abcam ab208670)

Phagocytosis assay

THP-1 macrophages were treated with either hCitH3-mAb or human IgG (control) at a concentration of 1.5 μg/mL. Following treatment, cells were exposed to *P. aeruginosa* at a multiplicity of infection (MOI) of 100 for 1 h to simulate bacterial stress. Following infection, cells were incubated with pHrodo™ Red E. coli BioParticles (Thermo Fisher, P35360) at 0.1 mg/mL for 30 min at 37 °C to assess phagocytic function. The pHrodo dye fluoresces upon internalization into acidic compartments, enabling quantification of active phagocytosis. Nuclei were counterstained with Hoechst. Red fluorescence, indicating phagocytic uptake, was measured at excitation/emission wavelengths of 560/585 nm using a plate reader for quantification. Representative images were acquired to using a fluorescence microscope.

Live cell Ca^{2+} imaging

BMDM cells were loaded with Fluo-4-AM (2 μM) in 0 Ca^{2+} Krebs-Ringer Hepes buffer containing (mM) 125 NaCl, 5 KCl, 25 HEPES, 6 glucose, and 1.2 $MgCl_2$, pH 7.4 for 40 min at room temperature. Cells were then continuously perfused with Krebs-Ringer Hepes (KRH) solution containing $CaCl_2$ (1.8 mM) at room temperature. Fluorescence of Fluo-4 was excited at 488 nm and detected by a Nikon A1R confocal microscope. For measurements of $[Ca^{2+}]_i$ response, BMDMs were treated with 20 μg/ml CitH3 or H3 peptides in KRH buffer and monitored continuously under the microscope.

Cell viability assay (CCK-8)

Cell viability was assessed using the Cell Counting Kit-8 (CCK-8, Dojindo, CK04) according to the manufacturer's protocol. Briefly, cells were seeded into 96-well plates at a density of 1×10^4 cells per well and allowed to adhere overnight. Following specific treatments, 10 μL of CCK-8 solution mixed with 100 μL of culture media (without phenol red) was added to each well. Absorbance was measured at 450 nm. Cell viability was expressed as a percentage relative to the untreated control group. Data were normalized to the control group, and statistical analyses were performed as described in the corresponding sections.

Cell death assay

Cell death in THP-1 cells was assessed using the Cell Death Detection ELISA kit (Roche, 11544675001) according to the manufacturer's instructions. THP-1 cells were cultured in 96-well plates at a density of 1×10^6 cells per well and treated under specified experimental conditions. Following treatment, cells were lysed using the kit's lysis buffer to release cytoplasmic histone-associated DNA fragments. The lysates were transferred to a streptavidin-coated microplate and incubated with a biotinylated anti-histone antibody and a peroxidase-conjugated anti-DNA antibody. After washing to remove unbound antibodies, substrate solution was added to develop a colorimetric signal proportional to the amount of DNA-histone complexes. Absorbance was measured at 405 nm using a microplate reader to quantify cell death, and data were normalized to untreated controls.

Antibody-dependent cellular cytotoxicity (ADCC) reporter assay

The day before assay, PD-L1-overexpressing (PDL1-OE) THP-1 cells were harvested from continuous culture by centrifugation and resuspended in cell culture medium containing 10% FBS and 100 ng/mL PMA at a final density of 1.25×10^4 cells/well in 96-well assay plates. 16 h later, PDL1-OE THP-1 cells were differentiated into macrophage-like cells. Cell culture medium was replaced with 1:3 serial dilutions of human IgG1, anti-PDL1, and hCitH3-mAb antibodies. For dilution, hCitH3 sample (20 mg/mL) was diluted with 1X PBS to a stock solution of 2 mg/mL; samples were subjected to 3-fold serial dilutions with ADCC Assay Buffer. According to the manufacturer's instructions (Promega, ADCC Reporter Bioassay Core Kit, Cat #ADG7941), effector cells (Jurkat T cells) were then added at 7.5×10^4 cells/well and incubated at 37 °C for 6 h. After incubation, assay plates were removed from the 37 °C incubator and allowed to equilibrate to ambient temperature (22–25 °C) on the bench for 15 min. 75 μl of Bio-Glo™ Luciferase Assay Reagent was added to the assay plates and incubated at ambient temperature for 10 min. Luminescence counts were recorded using a plate reader. Data analysis was performed using Log (Agonist) vs. response – Variable slope program of GraphPad Prism Software Version 5.

LDH release assay

Cytotoxicity was evaluated by measuring lactate dehydrogenase (LDH) release using the LDH Cytotoxicity Detection Kit (Sigma-Aldrich, 11644793001). Cells were seeded in a 96-well plate at a density of 1×10^4 cells per well and allowed to adhere overnight. After specific treatments, 50 μl of cell culture supernatant from each well was transferred to a new 96-well plate. To measure maximum LDH release, cells in positive control wells were lysed with 0.2% Triton X-100. LDH reaction mixture (50 μL) was added to each sample well and incubated at room temperature in the dark for 10 min, following the manufacturer's protocol. Absorbance was measured at 490 nm with a reference wavelength of 600 nm. LDH release was expressed as a percentage of the maximum LDH release (Triton group). All data were normalized to the control group for analysis.

Neutral red assay

Neutral Red (NR) assay was performed to assess cell viability and cytotoxicity using the Neutral Red Assay Kit (Sigma, TOX4-1KT). Cells were seeded in a 96-well plate and treated with the desired compounds for a specified duration. Following treatment, cells were incubated with Neutral Red solution (provided in the kit) for 3 h at 37 °C to allow for uptake into viable cells. After incubation, cells were washed to remove excess dye, and the incorporated Neutral Red was eluted with a lysis buffer. Absorbance was measured at 540 nm using a microplate reader, and cell viability was calculated relative to untreated control cells.

dsDNA release for NETosis quantification

Primary neutrophils were isolated from mouse bone marrow and seeded into 96-well plates at a density of 2×10^5 cells per well. Cells were treated with CitH3 peptides (5 μg/mL) and the CitH3 antibodies (5 μg/mL), and samples were collected at various time points over a 0–6-hour period to assess NETosis. To quantify dsDNA release, the Quant-iT™ PicoGreen™ dsDNA Assay Kit (Invitrogen, P7581) was used according to the manufacturer's instructions. After treatment, supernatants were collected and mixed with the PicoGreen™ reagent in black, flat-bottom 96-well plates. Fluorescence was measured using a microplate reader with excitation/emission wavelengths of 480/520 nm. Data were normalized to a 0.1% Triton X-100-treated group as the positive control.

Enzyme-linked immunosorbent assay (ELISA)

For direct ELISA in Supplementary Fig. 1, all the CitH3 antibodies were conjugated with HRP following the protocol of a kit (Abcam, ab102890). Different dose of CitH3 peptide were directly coated onto 96-well plates overnight at 4 °C. Different concentrations of CitH3 peptide were coated directly onto 96-well plates overnight at 4 °C. After blocking for 2 h, the CitH3 antibodies (0.1 μg/mL) were added and incubated for 2 h at room temperature. TMB was used as the substrate.

CitH3 levels in Fig. 2, 3 and traditional ELISA of CitH3 in Supplementary Fig. 3 were determined using an indirect ELISA. Briefly, hCitH3-mAb or commercial CitH3-mAb (5 μg/mL) was coated onto 96-well plates overnight at 4 °C. After blocking for 2 h, samples were added and incubated overnight at 4 °C. Following sample incubation, a CitH3 detection antibody (Abcam, ab5103, USA) was applied for 2 h at room temperature, followed by incubation with an HRP-conjugated secondary antibody for 1 h. TMB was used as the substrate. Absorbance was measured at 450 nm after substrate addition, providing a quantitative assessment of CitH3 levels in the samples. The commercial antibodies are as follows: Cayman mAb (17939); MyBiosource mAb (MBS483041); CST mAb (97272); AbboMax pAb (630-180ABBOMAX); and Abcam pAb (ab5103). Cytokine levels in bronchoalveolar lavage fluid (BALF) and cell supernatants were measured by the Immunology Core Facility at the University of Michigan.

In vitro citrullination assay and detection of citrullination

In vitro citrullination assay was performed as we previously described in refs. 52,53. Briefly, recombinant human H3 (Cayman, 10263) or His-tagged recombinant human PAD2 (Cayman, 10785) were incubated with MBP-tagged recombinant human PAD2 (Sigma-Aldrich, SAE0061) in a reaction buffer (50 mM HEPES, 50 mM NaCl, 2 mM $CaCl_2$, 2 mM DTT) or a Ca^{2+}-free reaction buffer containing EGTA for Ca^{2+} chelation at 37 °C for 4 h. To evaluate the impact of PAD4 on PAD2 citrullination, recombinant human PAD4 (Sigma-Aldrich, SAE0086) was added to the reaction system. Following incubation, proteins were treated with 0.1 mM citrulline-specific biotin-probe (PG-biotin, Cayman, 17450) in a buffer (50 mM HEPES, 20% trichloroacetic acid) at 37 °C for 30 min as previously described[54]. PG-biotin-labeled citrullinated proteins were captured using streptavidin-agarose beads (Thermo Fisher, 20353) and incubated overnight at 4 °C[53]. The bead-bound complexes were washed four times with PBS and boiled in SDS-PAGE sample buffer. The captured proteins were then analyzed by western blotting.

Western blot

Cells were collected and lysed using RIPA lysis buffer (Thermo Fisher, 89901) supplemented with a protease inhibitor cocktail (Thermo Fisher, 87785). For nuclear and cytoplasmic protein separation, the NE-PER™ Nuclear and Cytoplasmic Extraction Reagents (Thermo Fisher, 78835) were used following the manufacturer's protocol. Western blotting of the CitH3 peptide was performed using the Tris-Tricine SDS-PAGE system. Proteins were separated by Tris-Glycine SDS-PAGE and transferred to PVDF membranes. Membranes were blocked with 5% non-fat milk in PBST for 1 h at room temperature. Primary antibodies were applied overnight at 4 °C, followed by incubation with secondary antibodies (Jackson ImmunoResearch, USA) for 1 h at room temperature. After washes with PBST, protein bands were visualized using an ECL detection system (Bio-Rad, USA) and imaged with ChemiDoc Imaging Systems (Bio-Rad, USA).

Primary antibodies are: hCitH3-mAb, commercial CitH3-mAb (Cayman, 17939), PAD2 Ab (Proteintech, 12110-1), H3 Ab (Cell Signaling Technology, 9715S), β-actin Ab (Cell Signaling Technology, 4970S, 3700S), Citrulline Ab (Cayman, 30773), Caspase-1 (Cell Signaling Technology, 24232), PAD4 Ab (Abcam, ab214810), His-tag Ab (Proteintech, 66005-1-Ig), Cleaved Caspase-1 (Cell Signaling Technology, 89332), GSDMD (Cell Signaling Technology, 39754), Cleaved GSDMD (Cell Signaling Technology, 34667), GADPH (Cell Signaling Technology, 97166).

Statistical analysis

Data are presented as mean ± standard deviation (SD). For comparisons between two groups, a t-test was used. Repeated measures were analyzed using analysis of variance (ANOVA). For comparisons involving three or more groups, one-way or two-way ANOVA was performed as appropriate. Statistical analyses were conducted using Kaplan-Meier Analysis for survival rate. A p-value of <0.05 was considered statistically significant. Figures were analyzed using ImageJ 1.54 m, and statistical analysis was performed using GraphPad Prism 10.2.3.

Reporting summary

Further information on research design is available in the Nature Portfolio Reporting Summary linked to this article.

Data availability

The authors declare that the data supporting the findings of this study are available within the paper and its supplementary information files. The Source data that support the findings of this study are available in Figshare with the data "https://doi.org/10.6084/m9.figshare.29640344. Source data are provided with this paper.

References

1. Singer, M. et al. The Third International Consensus Definitions for Sepsis and Septic Shock (Sepsis-3). *JAMA* **315**, 801–810 (2016).
2. Angus, D. C. & van der Poll, T. Severe sepsis and septic shock. *N. Engl. J. Med* **369**, 2063 (2013).
3. Marshall, J. C. Inflammation, coagulopathy, and the pathogenesis of multiple organ dysfunction syndrome. *Crit. Care Med* **29**, S99–S106 (2001).
4. Prescott, H. C. & Angus, D. C. Enhancing Recovery From Sepsis: A Review. *JAMA* **319**, 62–75 (2018).
5. Hotchkiss, R. S., Monneret, G. & Payen, D. Sepsis-induced immunosuppression: from cellular dysfunctions to immunotherapy. *Nat. Rev. Immunol.* **13**, 862–874 (2013).
6. Rittirsch, D., Flierl, M. A. & Ward, P. A. Harmful molecular mechanisms in sepsis. *Nat. Rev. Immunol.* **8**, 776–787 (2008).
7. van der Poll, T., Shankar-Hari, M. & Wiersinga, W. J. The immunology of sepsis. *Immunity* **54**, 2450–2464 (2021).
8. Cavaillon, J. M. & Adib-Conquy, M. Monocytes/macrophages and sepsis. *Crit. Care Med* **33**, S506–S509 (2005).
9. Shi, J. et al. Inflammatory caspases are innate immune receptors for intracellular LPS. *Nature* **514**, 187–192 (2014).
10. Yipp, B. G. et al. Infection-induced NETosis is a dynamic process involving neutrophil multitasking in vivo. *Nat. Med* **18**, 1386–1393 (2012).
11. Papayannopoulos, V. Neutrophil extracellular traps in immunity and disease. *Nat. Rev. Immunol.* **18**, 134–147 (2018).
12. Brinkmann, V. et al. Neutrophil extracellular traps kill bacteria. *Science* **303**, 1532–1535 (2004).
13. Urban, C. F., Reichard, U., Brinkmann, V. & Zychlinsky, A. Neutrophil extracellular traps capture and kill Candida albicans yeast and hyphal forms. *Cell Microbiol* **8**, 668–676 (2006).
14. Saitoh, T. et al. Neutrophil extracellular traps mediate a host defense response to human immunodeficiency virus-1. *Cell Host Microbe* **12**, 109–116 (2012).
15. Abi Abdallah, D. S. et al. Toxoplasma gondii triggers release of human and mouse neutrophil extracellular traps. *Infect. Immun.* **80**, 768–777 (2012).
16. Branzk, N. et al. Neutrophils sense microbe size and selectively release neutrophil extracellular traps in response to large pathogens. *Nat. Immunol.* **15**, 1017–1025 (2014).
17. Narasaraju, T. et al. Excessive neutrophils and neutrophil extracellular traps contribute to acute lung injury of influenza pneumonitis. *Am. J. Pathol.* **179**, 199–210 (2011).
18. Akk, A., Springer, L. E. & Pham, C. T. Neutrophil Extracellular Traps Enhance Early Inflammatory Response in Sendai Virus-Induced Asthma Phenotype. *Front Immunol.* **7**, 325 (2016).
19. Saffarzadeh, M. et al. Neutrophil extracellular traps directly induce epithelial and endothelial cell death: a predominant role of histones. *PLoS One* **7**, e32366 (2012).

20. Thomas, G. M. et al. Extracellular DNA traps are associated with the pathogenesis of TRALI in humans and mice. *Blood* **119**, 6335–6343 (2012).
21. Savchenko, A. S. et al. VWF-mediated leukocyte recruitment with chromatin decondensation by PAD4 increases myocardial ischemia/reperfusion injury in mice. *Blood* **123**, 141–148 (2014).
22. Huang, H. et al. Damage-associated molecular pattern-activated neutrophil extracellular trap exacerbates sterile inflammatory liver injury. *Hepatology* **62**, 600–614 (2015).
23. Wynn, T. A., Chawla, A. & Pollard, J. W. Macrophage biology in development, homeostasis and disease. *Nature* **496**, 445–455 (2013).
24. Cookson, B. T. & Brennan, M. A. Pro-inflammatory programmed cell death. *Trends Microbiol* **9**, 113–114 (2001).
25. Karakike, E. & Giamarellos-Bourboulis, E. J. Macrophage Activation-Like Syndrome: A Distinct Entity Leading to Early Death in Sepsis. *Front Immunol.* **10**, 55 (2019).
26. Tessarz, P. & Kouzarides, T. Histone core modifications regulating nucleosome structure and dynamics. *Nat. Rev. Mol. Cell Biol.* **15**, 703–708 (2014).
27. Wu, Z. et al. Peptidylarginine Deiminase 2 in Host Immunity: Current Insights and Perspectives. *Front Immunol.* **12**, 761946 (2021).
28. Liu, X. et al. PAD4 takes charge during neutrophil activation: Impact of PAD4 mediated NET formation on immune-mediated disease. *J. Thromb. Haemost.* **19**, 1607–1617 (2021).
29. Pan, B. et al. CitH3: a reliable blood biomarker for diagnosis and treatment of endotoxic shock. *Sci. Rep.* **7**, 8972 (2017).
30. Poles, M. Z. et al. Kynurenic Acid and Its Synthetic Derivatives Protect Against Sepsis-Associated Neutrophil Activation and Brain Mitochondrial Dysfunction in Rats. *Front Immunol.* **12**, 717157 (2021).
31. Tian, Y. et al. Serum citrullinated histone H3 concentrations differentiate patients with septic verses non-septic shock and correlate with disease severity. *Infection* **49**, 83–93 (2021).
32. Nakashima, K., Hagiwara, T. & Yamada, M. Nuclear localization of peptidylarginine deiminase V and histone deimination in granulocytes. *J. Biol. Chem.* **277**, 49562–49568 (2002).
33. Wang, Y. et al. Human PAD4 regulates histone arginine methylation levels via demethylimination. *Science* **306**, 279–283 (2004).
34. Zheng, L. et al. Calcium Regulates the Nuclear Localization of Protein Arginine Deiminase 2. *Biochemistry* **58**, 3042–3056 (2019).
35. Jang, B. et al. Subcellular localization of peptidylarginine deiminase 2 and citrullinated proteins in brains of scrapie-infected mice: nuclear localization of PAD2 and membrane fraction-enriched citrullinated proteins. *J. Neuropathol. Exp. Neurol.* **70**, 116–124 (2011).
36. Cherrington, B. D. et al. Potential role for PAD2 in gene regulation in breast cancer cells. *PLoS One* **7**, e41242 (2012).
37. Wu, Z. et al. Peptidylarginine Deiminases 2 Mediates Caspase-1-Associated Lethality in *Pseudomonas aeruginosa* Pneumonia-Induced Sepsis. *J. Infect. Dis.* **223**, 1093–1102 (2021).
38. Zhou, J. et al. Peptidylarginine Deiminase 2 Knockout Improves Survival in hemorrhagic shock. *Shock* **54**, 458–463 (2020).
39. Wu, Z. et al. Inhibition of PAD2 Improves Survival in a Mouse Model of Lethal LPS-Induced Endotoxic Shock. *Inflammation* **43**, 1436–1445 (2020).
40. Deng, Q. et al. Citrullinated Histone H3 as a Therapeutic Target for Endotoxic Shock in Mice. *Front Immunol.* **10**, 2957 (2019).
41. Tian, Y. et al. Citrullinated Histone H3 Mediates Sepsis-Induced Lung Injury Through Activating Caspase-1 Dependent Inflammasome Pathway. *Front Immunol.* **12**, 761345 (2021).
42. Zhang, X. et al. Peptidylarginine deiminase 2-catalyzed histone H3 arginine 26 citrullination facilitates estrogen receptor alpha target gene activation. *Proc. Natl Acad. Sci. USA* **109**, 13331–13336 (2012).
43. Neeli, I. & Radic, M. Current Challenges and Limitations in Antibody-Based Detection of Citrullinated Histones. *Front Immunol.* **7**, 528 (2016).
44. Tian, Y. et al. Peptidylarginine deiminase 2 has potential as both a biomarker and therapeutic target of sepsis. *JCI Insight* **5**. https://doi.org/10.1172/jci.insight.138873 (2020).
45. Meyer, N. J. & Prescott, H. C. Sepsis and Septic Shock. *N. Engl. J. Med* **391**, 2133–2146 (2024).
46. Song, Y. et al. Rapid single-molecule digital detection of protein biomarkers for continuous monitoring of systemic immune disorders. *Blood* **137**, 1591–1602 (2021).
47. Song, Y. et al. A digital protein microarray for COVID-19 cytokine storm monitoring. *Lab Chip* **21**, 331–343 (2021).
48. Song, Y. et al. Machine learning-based cytokine microarray digital immunoassay analysis. *Biosens. Bioelectron.* **180**, 113088 (2021).
49. Kim, S. W., Lee, H., Lee, H. K., Kim, I. D. & Lee, J. K. Neutrophil extracellular trap induced by HMGB1 exacerbates damages in the ischemic brain. *Acta Neuropathol. Commun.* **7**, 94 (2019).
50. Zeng, F. L. et al. Neutrophil extracellular traps promote acetaminophen-induced acute liver injury in mice via AIM2. *Acta Pharm. Sin.* **45**, 1660–1672 (2024).
51. Kim, S. W. et al. Adenosine Triphosphate Accumulated Following Cerebral Ischemia Induces Neutrophil Extracellular Trap Formation. *Int. J. Mol. Sci.* **21**. https://doi.org/10.3390/ijms21207668 (2020).
52. Pitter, M. R. et al. PAD4 controls tumor immunity via restraining the MHC class II machinery in macrophages. *Cell Rep.* **43**, 113942 (2024).
53. Bicker, K. L., Subramanian, V., Chumanevich, A. A., Hofseth, L. J. & Thompson, P. R. Seeing citrulline: development of a phenylglyoxal-based probe to visualize protein citrullination. *J. Am. Chem. Soc.* **134**, 17015–17018 (2012).
54. Li, Y. et al. Citrullinated histone H3: a novel target for the treatment of sepsis. *Surgery* **156**, 229–234 (2014).
55. Fu, Q. et al. miR-155 enhances apoptosis of macrophage through suppressing PI3K-AKT activation in *Pseudomonas aeruginosa* keratitis. *Heliyon* **10**, e36585 (2024).
56. Ming, S. et al. Immunoglobulin-Like Transcript 5 Inhibits Macrophage-Mediated Bacterial Killing and Antigen Presentation During Sepsis. *J. Infect. Dis.* **220**, 1688–1699 (2019).
57. Qu, W. et al. Triggering Receptors Expressed on Myeloid Cells 2 Promotes Corneal Resistance Against *Pseudomonas aeruginosa* by Inhibiting Caspase-1-Dependent Pyroptosis. *Front Immunol.* **9**, 1121 (2018).
58. McClellan, S. A., Jerome, A., Suvas, S. & Hazlett, L. D. NLRC4 regulates caspase-1 and IL-1beta production in a CD11blowLy6Glow population of cells required for resistance to *Pseudomonas aeruginosa* keratitis. *PLoS One* **12**, e0185718 (2017).
59. Aoyagi, T. et al. Interleukin-36gamma and IL-36 receptor signaling mediate impaired host immunity and lung injury in cytotoxic *Pseudomonas aeruginosa* pulmonary infection: Role of prostaglandin E2. *PLoS Pathog.* **13**, e1006737 (2017).
60. Yu, F. S. et al. Flagellin stimulates protective lung mucosal immunity: role of cathelicidin-related antimicrobial peptide. *J. Immunol.* **185**, 1142–1149 (2010).
61. Stack, J. et al. TRAM is required for TLR2 endosomal signaling to type I IFN induction. *J. Immunol.* **193**, 6090–6102 (2014).
62. Soni, C. et al. Cutting Edge: TLR2 Signaling in B Cells Promotes Autoreactivity to DNA via IL-6 Secretion. *J. Immunol.* **211**, 1475–1480 (2023).
63. Fang, L., Wu, H. M., Ding, P. S. & Liu, R. Y. TLR2 mediates phagocytosis and autophagy through JNK signaling pathway in Staphylococcus aureus-stimulated RAW264.7 cells. *Cell Signal* **26**, 806–814 (2014).

64. Ding, R., Xu, G., Feng, Y., Zou, L. & Chao, W. Lipopeptide PAM3CYS4 Synergizes N-Formyl-Met-Leu-Phe (fMLP)-Induced Calcium Transients in Mouse Neutrophils. *Shock* **50**, 493–499 (2018).
65. Ma, D., Marey, M. A., Shimada, M. & Miyamoto, A. Toll-like Receptor 2 is Involved in Calcium Influx and Acrosome Reaction to Facilitate Sperm Penetration to Oocytes During in vitro Fertilization in Cattle. *Front Cell Dev. Biol.* **10**, 810961 (2022).
66. Ratner, A. J. et al. Cystic fibrosis pathogens activate Ca2+-dependent mitogen-activated protein kinase signaling pathways in airway epithelial cells. *J. Biol. Chem.* **276**, 19267–19275 (2001).
67. Chun, J. & Prince, A. Activation of Ca2+-dependent signaling by TLR2. *J. Immunol.* **177**, 1330–1337 (2006).
68. Yipp, B. G. & Kubes, P. NETosis: how vital is it?. *Blood* **122**, 2784–2794 (2013).
69. Lood, C. et al. Neutrophil extracellular traps enriched in oxidized mitochondrial DNA are interferogenic and contribute to lupus-like disease. *Nat. Med* **22**, 146–153 (2016).
70. Vander Cruyssen, B. et al. Anti-citrullinated protein/peptide antibodies (ACPA) in rheumatoid arthritis: specificity and relation with rheumatoid factor. *Autoimmun. Rev.* **4**, 468–474 (2005).
71. Trier, N. H. & Houen, G. Anti-citrullinated protein antibodies as biomarkers in rheumatoid arthritis. *Expert Rev. Mol. Diagn.* **23**, 895–911 (2023).
72. Lin, M. et al. Cyasterone ameliorates sepsis-related acute lung injury via AKT (Ser473)/GSK3beta (Ser9)/Nrf2 pathway. *Chin. Med* **18**, 136 (2023).
73. Gao, Z. et al. Machine-Learning-Assisted Microfluidic Nanoplasmonic Digital Immunoassay for Cytokine Storm Profiling in COVID-19 Patients. *ACS Nano* **15**, 18023–18036 (2021).

Acknowledgements

This work was supported by Joint-of-Institute Grant (Grant# U068874) to Y.L., and by the National Institutes of Health (NIH) grants R01HL155116 to Y.L., R01HL157215, R01AG07240 and R01EY036243 to JM and R35GM136312 to KAS. The authors acknowledge Dr. Yufang Shao and the Bon Opus Biosciences team for their excellent technical help during the early studies, and Dr. Yue Liu for the AI-based humanization of the CitH3-mAb. The content is solely the responsibility of the authors and does not necessarily represent the official views of the National Heart, Lung and Blood Institute, the National Institute on Aging, the National Eye Institute, the National Institute of General Medical Sciences or NIH.

Author contributions

Y.L. and J.M.: Conceptualization, writing – review & editing; W.O., Y.C.: Writing – original draft, data curation, investigation and methodology. T.T., Y.S., T.D., K.E.L., X.Z., Z.T., S.G., X.Y., L.S., C.Q., T.Z.: data collection and analysis. H.J., J.Q., Jichun Ma, B.W., Q.L., and G.D.Z.: Scale-up production of hCitH3-mAb. H.B.A., Y.T., Y.S., K.K., K.A.S.: Human samples and PEdELISA. Writing- Reviewing and Editing - all authors.

Competing interests

Patent application related to the hCitH3-mAb technology was filed by University of Virginia Patent Foundation, The Reagents of University of Michigan and HTIC, Inc. J.M., Y.L. and T.T. are co-founders of HTIC that develops hCitH3-mAb for immune modulation applications. The remaining authors declare no competing interests.

Additional information

Supplementary information The online version contains supplementary material available at https://doi.org/10.1038/s41467-025-62788-6.

Correspondence and requests for materials should be addressed to Yongqing Li or Jianjie Ma.

Peer review information *Nature Communications* thanks the anonymous reviewers for their contribution to the peer review of this work. A peer review file is available.

Reprints and permissions information is available at http://www.nature.com/reprints

Publisher's note Springer Nature remains neutral with regard to jurisdictional claims in published maps and institutional affiliations.

[1]Department of Surgery, University of Michigan Health System, Ann Arbor, MI, USA. [2]Department of Endocrinology and Metabolism, The Second Xiangya Hospital, Changsha, China. [3]Division of Surgical Sciences, Department of Surgery, University of Virginia, Charlottesville, VA, USA. [4]Department of Mechanical and Aerospace Engineering, NYU Tandon School of Engineering, Brooklyn, NY, USA. [5]Department of Mechanical Engineering, University of Michigan, Ann Arbor, MI, USA. [6]Department of Physiology, Xuzhou Medical University, Xuzhou, Jiangsu, China. [7]Department of Emergency Medicine, Second Affiliated Hospital, Zhejiang University School of Medicine, Hangzhou, Zhejiang, China. [8]Department of Urology, The Xiangya Hospital, Changsha, China. [9]Department of Pathology, Massachusetts General Hospital, Harvard Medical School, Boston, MA, USA. [10]Department of Rheumatology and Immunology, Xiangya Hospital, Changsha, China. [11]Department of Chemical and Biomolecular Engineering, New York University, Brooklyn, NY, USA. [12]SparX Biopharmaceutical Corp, Mount Prospect, IL, USA. [13]Department of Surgery, Northwestern University, Arkes Pavilion, Chicago, IL, USA. [14]Department of Clinical Pharmacy, College of Pharmacy, University of Michigan, Ann Arbor, MI, USA. [15]Division of Pulmonary and Critical Care Medicine, Department of Internal Medicine, University of Michigan School of Medicine, Ann Arbor, MI, USA. [16]The Max Harry Weil Institute for Critical Care Research and Innovation, University of Michigan, Ann Arbor, MI, USA. ✉e-mail: yqli@med.umich.edu; Jianjie.ma@virginia.edu